Biomaterials 185 (2018) 155–173

Contents lists available at ScienceDirect

Biomaterials

journal homepage: www.elsevier.com/locate/biomaterials

Bioinstructive microparticles for self-assembly of mesenchymal stem Cell-3D tumor spheroids

L.P. Ferreira, V.M. Gaspar*, J.F. Mano*

Department of Chemistry, CICECO – Aveiro Institute of Materials, University of Aveiro, Campus Universitário de Santiago, 3810-193, Aveiro, Portugal

ARTICLE INFO

Keywords:
3D *In vitro* tumor models
Co-culture
Bioinstructive microparticles
Drug screening
Lung cancer
Mesenchymal stem cells

ABSTRACT

3D multicellular tumor spheroids (3D-MCTS) that closely mimic *in vitro* the complex lung tumor microenvironment (TME) are highly desirable for screening innovative anti-cancer therapeutics. Despite significant improvements in mimicking lung TME, few models have combined tumor-infiltrating mesenchymal stem cells from bone marrow (hBM-MSCs) with heterotypic 3D tumor spheroid models containing ECM mimetic components. Herein, we engineered hybrid 3D-MCTS that combine, for the first time, A549:fibroblasts:hBM-MSCs in heterotypic tri-culture, with bioinstructive hyaluronan microparticles that act as tumor-ECM mimetics and as cell-anchoring hotspots. The obtained results indicated that 3D microspheres provided proper support for cells to self-assemble into compact 3D microtissues and promoted an increase in CD44 expression, emulating the presence of native-ECM hyaluronan. 3D-MCTS size and sphere-like morphology was reproducible and tri-culture models presented the characteristic solid tumors necrotic core. Mesenchymal stem cells tracking demonstrated that hBM-MSCs migrate to different regions in 3D microtumors mass exhibiting dynamic interactions with cancer cells and stromal fibroblasts, alike in human tumors. Importantly, doxorubicin administration revealed hBM-MSCs effect on cytotoxic responses in 3D tri-culture models and in dual cultures of hBM-MSCs:A549 at 10:1 ratio. Such findings evidence the relevance of including hBM-MSCs in combination with cancer-stromal fibroblasts in 3D *in vitro* tumor models and the importance to test different cell-to-cell ratios to mimic tumor heterogeneity. In addition, bioinstructive hyaluronan-microparticles were also effective as cell-agglomerating scaffolds and showed potential to be used as an enabling technology for including different ECM components in 3D *in vitro* models in the future.

1. Introduction

Presently, *in vitro* preclinical validation platforms recommended by regulatory agencies to screen for candidate anti-cancer therapeutics are mainly based on the use of 2D cell monolayers and *in vivo* animal models [1,2]. Both of these are increasingly seen as inadequate approximations of the complex human tumor microenvironment (TME) [3,4]. 2D monocultures are unable to correctly recapitulate spatial organization, cell-cell and cell-matrix interactions, biochemical cues and TME heterogeneity [5]. While animal models are recognizably expensive, laborious and ethically controversial alternatives, often lacking correct representation of the human tumor stroma or tumor infiltrating immune system [6,7]. Improved representation of the TME in *in vitro* tumor mimicking platforms is urgent for improving basic cancer biology research (e.g., new biomarkers and biological targets) and drug-screening procedures.

Three-dimensional multicellular tumor spheroids (3D-MCTS) currently receive an increased attention in the field of anti-cancer drug discovery due to their ability to robustly recapitulate specific features of *in vivo* tumors [8]. In fact, such models allow a straightforward cellular stroma representation by combination of malignant and non-malignant cell populations in a 3D environment that promotes cell-cell contacts and communication [9]. Cells cultured in 3D self-aggregate to form *in vitro* microtissues that mimic oxygen/nutrient and pH gradients of human solid tumors [10]. Such provides an *in vivo* surrogate environment in which cancer cells phenotypical, genetical and metabolical heterogeneity can be easily recapitulated. However, despite better portraying the diverse cellular components of tumor microenvironment (TME), in general 3D-MCTS lack pre-existing extracellular matrix (ECM) components, with ECM being deposited by cells during culture [11]. Inclusion of ECM-mimetics (e.g., hyaluronic acid [12], collagen [13], fibrinogen [14]), may improve 3D-MCTS ability to correctly

* Corresponding authors. Department of Chemistry, CICECO – Aveiro Institute of Materials, University of Aveiro, Campus Universitário de Santiago, 3810-193, Aveiro, Portugal.

E-mail addresses: vm.gaspar@ua.pt (V.M. Gaspar), jmano@ua.pt (J.F. Mano).

https://doi.org/10.1016/j.biomaterials.2018.09.007
Received 5 August 2018; Received in revised form 6 September 2018; Accepted 7 September 2018
Available online 13 September 2018
0142-9612/

mimic tumor specific-ECM at an early stage. This supportive matrix is known to influence the process of metastasis, invasion, and acquisition of multi-drug resistance [15].

Regarding lung cancer ECM, one key component that has been associated with poor patient prognosis is Hyaluronic acid (HyA) [16–18]. This biopolymer is comprised by disaccharides of D-glucuronic acid and *N*-acetyl-D-glucosamine is found ubiquitously in human tissues [19,20]. Several studies observed that cancer cells associated to a HyA-rich ECM environment exhibit an increased expression of two key cellular receptors: (i) CD44, a marker associated with multidrug resistance [21,22]; and (ii) RHAMM (receptor for hyaluronan-mediated motility, also known as cluster of differentiation 168 – CD168), a receptor associated with invasion and metastasis through changes in motility, polarity and directed migration, as well as involved in matrix remodeling proteins production (e.g., MMP-9 or PAI-1) [20]. Apart from this, also the cellular components of the TME must be included in the design of 3D *in vitro* tumor models so as fully recapitulate malignant-stromal cells heterogeneity.

In this context, human mesenchymal stem cells (MSCs) have been recently recognized as important cellular constituents of the TME playing paramount roles in multiple cancers [23–26]. MSCs have been involved in the: (i) regulation of the immune response [27,28], (ii) modification of the surrounding tumor-ECM [29,30], (iii) conversion of fibroblasts to CAFs [31], (iv) initiation of epithelial-to-mesenchymal transition (EMT) by cancer cells [32], and (v) metastasis [27]. Despite these contributions to cancer progression, some reports also emphasize MSCs role in inhibiting and suppressing tumor proliferation, invasion and metastasis [33]. The different influences of MSCs in lung cancer have been recently revised elsewhere [30]. Given their polyvalent activity, the representation of MSCs in 3D models is critical for the correct recapitulation of human tumors in an *in vitro* setting. However, to date, few works have explored MSCs inclusion in a ECM-containing 3D environment, and even fewer in a heterotypic model that includes the main populations of the TME (i.e., cancer cells and fibroblasts) [34].

From this standpoint, herein we designed a multicomponent 3D *in vitro* lung tumor model that simultaneously recapitulates TME cellular heterogeneity and cell-ECM crosstalk. The latter was accomplished by incorporation of poly(ε-caprolactone) microparticles (MPs) coated with a bioinstructive HyA multilayer produced via the layer-by-layer (LbL) deposition technique. Moreover, hBM-MSCs were also co-cultured with A549 cancer cells and fibroblasts for the first time in 3D to evaluate their influence in the response to chemotherapeutics. Overall the obtained results demonstrate that bioinstructive MPs promote the assembly of robust and reproducible 3D-MCTS and that the inclusion of hBM-MSCs must be considered in the design of *in vivo* mimicking 3D tumor models were the infiltration of these cells occurs (e.g., lung, breast, prostate, colorectal).

2. Materials and methods

2.1. Materials

Polycaprolactone (PCL; Mn: 80 000 Da), Polyvinyl Alcohol (PVA; MW: 30 000–70 000 Da) and Poly-L-lysine hydrobromide (PLL; MW: 30 000–70 000 Da) were acquired from Laborspirit (Loures, Portugal). Chitosan chloride (MW: 50 000–150 000 Da) was acquired from Novamatrix (Sandvika, Norway). Hyaluronic acid sodium salt polymer (MW: 80 000–100 000 Da) was purchased from Carbosynth Limited (Berkshire, United Kingdom). Ultra-Low-Adhesion (ULA) round-bottom 96-wells plates, Fetal Bovine Serum (FBS; E.U. approved, South America origin), Dulbecco's Modified Eagle Medium-High Glucose (DMEM-HG), phosphate buffered saline, pH = 7.4 without Ca^{2+} and Mg^{2+} (dPBS), Ham's F-12K Kaighn's Medium (HAMs-F12), Alpha Modified Eagle's Medium (α-MEM), TrypLE™ Express, Goat anti-Mouse IgG (H + L) Alexa Fluor 488 (Alexa 488) Secondary Antibody, anti-human Collagen I Antibody (5D8-G9), anti-human *E*-cadherin-PE antibody, Calcein-AM, Propidium Iodide (PI) were all purchased from Thermofisher Scientific Inc (Alfagene, Portugal). Anti-human CD44-FITC was purchased from Taper (Grupo Taper S.A., Lisboa, Portugal). All other reagents and salts were of analytical grade and used without further purification.

2.2. Methods

2.2.1. PCL microparticles production

PCL microparticles where produced by using the oil-in-water (O1/W1) emulsion-solvent evaporation technique. The oil phase (O1) was comprised by a 5% (w/v) PCL solution. The aqueous phase (W1) consisted of 0.5% (w/v) PVA aqueous solution. To form the water-oil emulsion 8 mL of PCL (O1 phase) were dispersed into 150 mL of PVA by using a high precision piezoelectric-based air pumping system (OB1 MK3 –Microfluidic Flow Control System, Elveflow®, France), operated at an air pressure of 5 bar. The microparticle-containing solution was then placed under horizontal stirring at 170 rpm during at least 8 h, at room temperature (RT), inside a fume-hood. The recovered PCL microparticles were washed 3 times with deionize water by using resuspension/centrifugation cycles (1000 rpm, 5 min). The particles were then sieved through stainless steel sieves to obtain particle size ranges from 63 μm to 100 μm. All particles were freeze dried for 48 h and stored in a moisture free atmosphere until further use.

2.2.2. Bioinstructive microparticles production via layer-by-layer

Prior to biopolymers surface functionalization microparticles were subjected to plasma treatment. For this purpose, 200 mg of sieved microparticles where placed in a sterile beaker and subjected to plasma treatment by using atmospheric air charged at 30 V, for 5 min, RT. For Layer-by-layer (LbL) surface functionalization 250 mg of plasma treated PCL MPs (LbL-MPs, negative charge), were then immersed in 20 mL of PLL (1 mg/mL, 0.22 μm filtered), for 10 min, and washed in distilled water for 5 min. For the buildup of the negative layer, PLL-MPs were transferred into an HyA solution (1 mg/mL, filtered 0.22 μm) for 10 min, and re-washed for 5 min. This process was repeated 3 times to allow the formation of 3 PLL/HyA bilayers.

2.2.3. Zeta potential analysis of polyelectrolyte polymers deposition

Zeta potential measurements were used to verify the buildup of polyelectrolyte layers in MPs surface during LbL. This analysis was also performed in plasma treated, non-coated, PCL MPs that were used as control. All measurements where performed in a ZetaSizer Nano ZS (Malvern, Worcestershire, UK), at 25 °C by using the automatic mode and a disposable cell (DTS1070). The ZetaSizer software was used to record and convert the electrophoretic mobility data to zeta potential (v. 7.04).

2.2.4. Microparticles characterization

Microparticles morphology and particle size was evaluated by optical contrast light microscopy (Primostar, Carl Zeiss, Germany). The acquired images where analyzed using open-source software ImageJ v1.08 (NIH, Bethesda, ML) [35] and microparticles size distribution was determined via a supervised algorithm that analyzed a minimum of 300 microparticles. Scanning Electron microscopy (SEM) imaging was used to analyze microparticle morphology and surface topography. For SEM analysis, were dispersed in deionized water and drop-wise added to an aluminum stub containing a glued tissue culture treated polystyrene insert (TCPS, Starstedt, Lisbon, Portugal). The samples were then dried at 37 °C overnight, sputter coated with gold/palladium and observed in a Hitachi S-4100 scanning electron microscope (Hitachi, Japan) operated at a voltage in the range of 15–25 kV and at various magnifications.

2.2.5. Cell culture

All cells were manipulated in aseptic conditions and cultured at

Table 1
Culture conditions tested for optimal spheroid formation.

Culture Type	Cell Lines	Cell-to-cell Ratios	Seeding Densities (Cell/well)	MPs Concentration (mg/well)	Ref[a]
Monoculture	A549	1	5000	0.0	[36]
Biculture	A549	1:2	10000	0.025	[37–40]
	HF		15000	0.050	
			30000		
			45000		
Biculture	A549 hBM-MSCs	10:1	15000	0.0	[30,41]
Triculture	A549	10:20:1	30000	0.025	[30,36–38,41,42]
	HF hBM-MSCs		45000		

[a] References describing cell-to-cell ratios.

37 °C in a humidified temperature-controlled incubator with a 5% CO_2 atmosphere. The non-small cell lung carcinoma cell line A549 (ATCC CRM-CCL-185™) was cultured in HAMs-F12 medium supplemented with 10% (v/v) FBS and 1% (v/v) ATB. The human primary dermal fibroblasts cell line (HF) (ATCC®-PCS-201-012™) was cultured in DMEM-HG supplemented with 10% (v/v) FBS and 1% (v/v) ATB. Huma adult Bone Marrow-derived Mesenchymal Stem Cells (hBM-MSCs) (ATCC®-PCS-500-012™) were cultured in α-MEM supplemented with 10% (v/v) FBS and 1% (v/v) ATB. All cells where detached from culture flasks upon attaining approximately 80–85% confluency by using TrypLE™ Express Enzyme (1×) detaching reagent. Throughout all studies hBM-MSCs were used from passage 3 to 7 to assure trilineage differentiation potential.

2.2.6. 3D In vitro lung tumor models assembly via liquid-overlay technique

Homotypic monoculture 3D-MCTS formed by A549 cells, heterotypic co-culture spheroids A549:HF and A549:hBM-MSCs cells, or tri-cocultures: A549:HF:hBM-MSCs cells, were self-aggregated at different cell ratios (Table 1), by using the liquid-overlay technique, also known as forced-floating methodology. To form 3D-MCTS cells were initially multiple or single-cell suspensions comprised by the different cell populations were cultured in ULA round bottom 96-wells plates. For 3D-MCTS hybrid spheroids cells were cultured with LbL-MPs. Prior to each assay, LbL-MPs were sterilized under UV light (30 min) and re-suspended in complete HAMs-F12 cell culture medium. To produce different 3D *in vitro* models that would better recapitulate tumor microenvironment cellular heterogeneity, different parameters were manipulated, namely: (i) the cell number per well, (ii) the cell-to-cell ratios between malignant and mesenchymal/endothelial cells and (iii) the cell-to-particle ratios. The specific ratios used for each condition are summarized in (Table 1).

2.2.7. 3D tumor microtissues characterization

3D *in vitro* hybrid spheroids morphology, growth and circularity were analyzed overtime via optical contrast microscopy by using an inverted microscope (Primovert, Carl Zeiss, Germany). Micrographs were acquired at specific timepoints (day 1, 7 and 14), and a minimum of 6 spheroids were analyzed per condition/time point. Image analysis was carried out by using the open-source software ImageJ (Fiji package) and a supervised algorithm based on the code developed by Ivanov and co-workers [43]. 3D *in vitro* tumor models' circularity was evaluated in ImageJ v1.08 (NIH, Bethesda, ML), as previously described in the literature [44]. Circularity was calculated from optical contrast microscopy images by using the following equation:

$$Circularity = 4\pi\left(\frac{area}{perimeter^2}\right) \quad (1)$$

For SEM analysis, 3D spheroids were processed as reported in the literature [37,45,46]. In brief, 3D-MCTS with and without LbL-MPs were removed from culture media and washed with dPBS, fixed in formaldehyde 4% (v/v, in dPBS), at 37 °C for 2 h. The samples were then subjected to dehydration with graded ethanol concentrations (25%, 50%, 75%, 90% (v/v)), for 20 min. All samples were then carefully mounted in aluminum stubs by using double sided adhesive carbon tape (Agar Scientific, Essex, United Kingdom) and sputter coated with gold/palladium. All spheroids were imaged in a scanning electron microscope (Hitachi S-4100), operated at different voltages and various magnifications.

2.2.8. Cell viability assays

The cell viability and necrotic core formation of different homotypic and heterotypic *in vitro* 3D microtumors (3D-MCTSs and 3D-MCTS LbL-MPs), were analyzed at specific timepoints (7 and 14 days) by using the Alamar Blue® Cell Viability Assay and Calcein-AM/PI, live/dead assay. Alamar blue was used to access 3D tumor model's viability during the initial steps of homotypic and heterotypic mono-, dual and tri-co-cultures optimization. Both assays were performed in accordance with manufacturer instructions. Alamar Blue (resazurin active compound), reduction to resorufin was determined by fluorescence measurements (λ_{ex}: 540 nm, λ_{em}: 600 nm). Fluorescence data was recorded in a Synergy HTX microplate reader by using a 96-well black-clear bottom plate.

2.2.9. 3D-MCTS characterization by widefield and confocal laser scanning fluorescence microscopy

The production of Collagen I was analyzed at specific timepoints (7 and 14 days) through immunocytochemistry. For this purpose, 3D-MCTS were fixed in 4% formaldehyde (v/v, in dPBS), overnight, at RT. The spheroids were then carefully transferred to a new 96 well ULA plate, washed and incubated for 1 h with blocking solution (1% BSA in dPBS), at 4 °C, followed by a washing step with dPBS. Then 3D-MCTS were incubated with *E*-cadherin-PE (5 μL/mL), or Collagen I (2.5 μL/mL) antibody overnight, at 4 °C, washed with dPBS for 3 times. Collagen I-stained spheroids where then incubated with Alexa488 secondary antibody for 1 h, RT. Acquisition of fluorescence micrographs was performed in an upright widefield microscope (Axio Imager M2, Carl Zeiss, Germany), or in laser scanning confocal microscopes (LSM 510 Meta, and LSM 880 Airyscan, Carl Zeiss, Germany). The analysis of acquired images was performed in Zeiss Zen Blue software (2017).

To evaluate 3D-MCTS necrotic core formation, the spheroids were labelled with Calcein-AM (Cal-AM) (4 μg/mL) and Propidium Iodide (PI) (10 μg/mL) for 30 min at 37 °C, according to literature reports for 3D models [37]. Following incubation, the different 3D tumor models (3D-MCTS and 3D-MCTS LbL-MPs) were washed 3 times with dPBS and imaged immediately by fluorescence microscopy.

2.2.10. Histological analysis

Histological analysis of dual co-culture (A549:HF) and tri-coculture (A549:HF:hBM-MSCs 3D-MCTS cultured in LbL-MPs was performed in order to analyze microtumors internal organization and collagen deposition. In brief, 3D-MCTS with and without LbL-MPs were removed from culture media and washed with dPBS, fixed in formaldehyde 4% (v/v, in dPBS), at 37 °C for 2 h. The samples were then subjected to

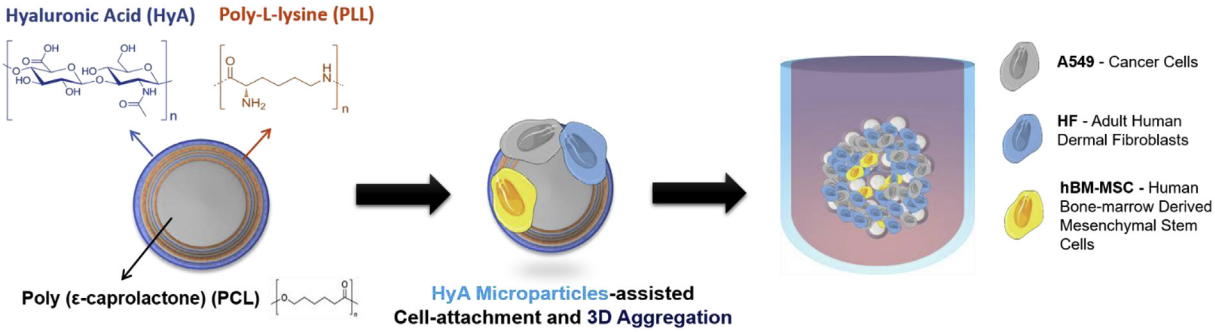

Fig. 1. Schematics of spherically structured 3D multicellular lung tumor models' assembly. The *in vitro* models are comprised by cancer cells, stromal fibroblasts and mesenchymal stem cells attached to bioinstructive, HyA-coated microparticles.

dehydration with growing concentrations of ethanol (25%, 50%, 75%, (v/v)), for 20 min, per condition. For histological analysis paraffin blocks containing 3D-MCTS were sliced into 5 μm thick samples and stained with: (i) Hematoxylin and Eosin (H&E), and (ii) Masson's Trichrome for evaluation of collagen deposition. Histology slides were then analyzed by using an inverted optical contrast light microscope (Primovert, Carl Zeiss, Germany) equipped with a 3Mpix color camera (Zeiss 105, Carl Zeiss, Germany). All images were acquired and processed in Zeiss Zen Blue Software (2017).

2.2.11. Flow cytometry analysis

The effect of hyaluronan bioinstructive LbL-MPs in 3D-MCTS CD44 expression was analyzed by flow cytometry. For this analysis, 3D-MCTS and 3D-MCTS LbL-MPs with 7 days of culture were dissociated by incubation in a 1:1 mixture of Accumax® and TrypLE™ Express for 30 min, at 37 °C. After this incubation period, spheroids were fully disrupted by gentle pipetting and incubated in HAMs-F12/10% FBS/1% ATB for 30 min and washed with dPBS for 3 times. The resulting single cells suspensions was then recovered by centrifugation. The different samples were incubated with anti-human CD44-FITC conjugate antibody (5 μL/mL in PBS) for 30 min, at 37 °C. Single cells were then recovered by centrifugation and washed with dPBS for 3 times. Prior to FCM analysis all samples were filtered through cell strainers (40 μm) to remove unbound particles. In addition, 2D monocultures of A549, HF and MSCs were also analyzed for their CD44 expression. Flow cytometry analysis was carried out in a BD Accuri C6 flow cytometer (BD Bioscience, San Diego, CA, USA) were a total of 5×10^3 events per sample were acquired in the ROI of interest. Flow cytometry data was processed and analyzed in FCS Express software (v. 6.0, trial license).

2.2.12. Chemotherapeutic drug cytotoxicity screening in 3D-MCTS platforms

Obtained 3D-MCTS were cultured for 7 days on HAMs-F12 medium to be used as testing platforms for Doxorubicin cytotoxicity evaluation in monotypic monocultures (A549 cells), heterotypic bi co-cultures (A549:HF), and triple co-cultures (A549:HF:hBM-MSCs). Upon achieving the desired culture time, 3D-MCTS were incubated with Doxorubicin (Dox) chemotherapeutic agent at different concentrations ranging from 0.7 to 17 μM, over a period of 72 h. Cellular viability of 3D-MCTS was then evaluated by using a luminescence-based assay specifically designed to quantify cellular ATP in *in vitro* 3D cellular aggregates assembled either via scaffold-based or scaffold free methods (Cell Titer Glo™ Luminescent cell viability assay, Promega, Madisson, WI, USA). CellTiter-Glo® assays were performed accordance with the manufacturer instructions. In brief, following incubation with Dox the medium was removed and 3D-MCTS were incubated with a mixture of HAMs-F12/10 %FBS/1% ATB medium and CellTiter-Glo® reagent at a 1:1 ratio. The samples were incubated for 25 min, at RT. Luminescence was then measured in 96-well flat-bottom opaque white plates by using a Synergy HTX microplate reader. Non-treated 3D-MCTS were used as controls.

2.2.13. Statistical analysis

All statistical analysis was performed using Graphpad Prism 6 Software (Prism 6™). One-way analysis of variance (One-ANOVA) and Two-way analysis of variance (Two-ANOVA) with Holm-Sidak's post-hoc test. A minimum of 6 replicates was used for statistical analysis. Unless otherwise indicated, $p < 0.05$ was considered statistically significant.

3. Results and discussion

The establishment of *in vitro* 3D microtumor models relevant for drug screening at preclinical discovery stages must emulate tumor cellular heterogeneity and biomacromolecular microenvironment, so as to provide a highly robust *in vitro/in vivo* correlation [47]. Currently, the great majority of 3D tumor models for *in vitro* drug screening are based on the use of scaffold-free cell-agglomerates, i.e., 3D spheroids. However, by definition, these models lack pre-existent tumor-ECM components, being a rather simplistic representation of the complex tumor microenvironment (TME) [8]. One approach to overcome such limitations is the inclusion of ECM-like scaffolds based on microparticles functionalized with bioinstructive tumor-ECM components (e.g., collagen, hyaluronan, etc) [48]. Microparticle technology has been extensively used in the field of tissue engineering due to their ability to support cell attachment, proliferation and promote a robust self-aggregation [49]. MPs co-cultured with different types of cells can also incorporate mechanical, biochemical and biomolecular tissue-specific cues.

As recently reviewed [50], few reports have explored microparticles as a strategy to include tumor-ECM mimetic components into spherical *in vitro* 3D tumor models. In general, microparticle-based 3D tumor models employ synthetic, non-bioinstructive microparticles. In this work LbL-MPs (63–100 μm) were used as a cost-effective and straightforward strategy to integrate virtually any ECM-mimetic substrates into *in vitro* assembled 3D-MCTS by using the LbL functionalization technology.

In the context of bioengineered *in vitro* tumor models, spherically-structured polymeric microparticles provide a unique surface for prompting rapid cells adhesion/aggregation, proliferation and for functionalization with tumor-ECM mimics. Taking advantage of this potential, we have developed a microparticle-based platform coated, via layer-by-layer (LbL), with a positive poly amino acid (Poly-L-Lysine) and negatively charged hyaluronan (HyA), a key component of tumor-ECM that provides adhesion hotspots to cells and also triggers important biochemical (Fig. 1). These so-termed bioinstructive microparticles (LbL-MPs) were then used as scaffolding platforms establish a unique tri-coculture model comprising A549 lung cancer cells, human

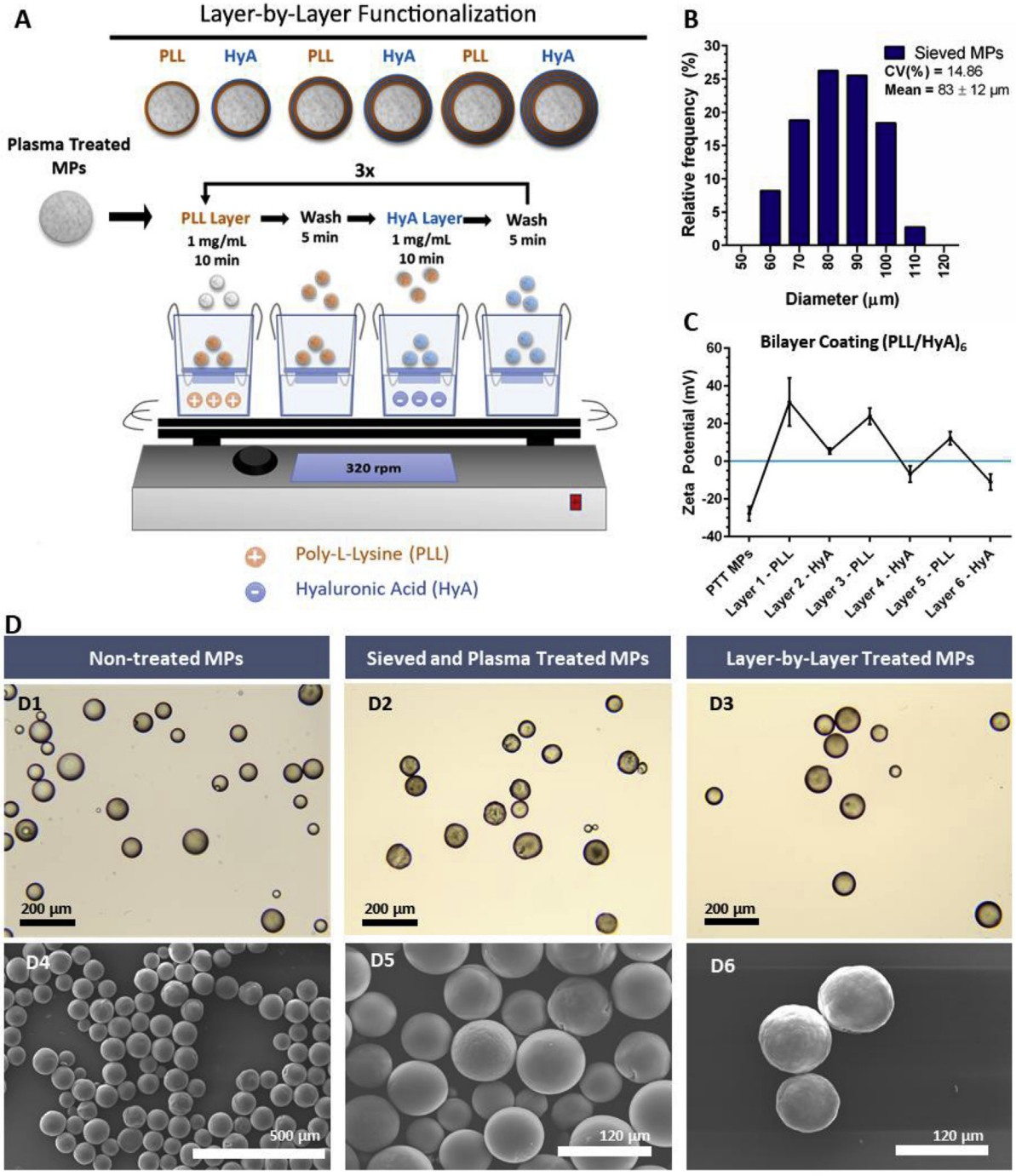

Fig. 2. Microparticles production and HyA biofunctionalization. (A) Schematic representation of layer-by-layer (LbL)-assisted microparticles biofunctionalization. (B) Characterization of PCL MPs size distribution after sieving. (C) Zeta potential analysis of MPs surface during sequential deposition of oppositely charged polyelectrolyte polymers. Data is represented as mean ± s.d, (n = 3). (D) Optical contrast microscopy and SEM micrographs of LbL PCL microparticles. (D1 and D4) Microparticles prior to plasma treatment; (D2 and D5) after plasma treatment; and (D3 and D6) following LbL treatment.

fibroblasts and bone marrow-derived mesenchymal stem cells (hBM-MSCs) (Fig. 1). The proposed multifactorial approach of this study aims to recapitulate the malignant-stromal cellular heterogeneity and provide a robust representation of the tumor microenvironment constituents. Up-to-date, very few studies have focused on the inclusion of MSCs in 3D *in vitro* tumor models [34]. As we recently reviewed, MSCs are an important element of *in vivo* human tumors, having diverse modulatory effects in tumors response to therapy, and should also be emulated *in vitro* [34]. Moreover, to the best of our knowledge, the present study is the first that includes stromal fibroblasts and mesenchymal stem cells in a 3D *in vitro* tumoral setting.

3.1. Microparticles production and layer-by-layer functionalization

Initially, the bioinstructive PCL-based MPs that served as structural platforms for 3D cells culture were formulated through the emulsion/solvent evaporation technique. The parameters influencing MPs production (polymer and surfactant concentration, oil-water solvent ratios, stirring), were optimized for efficient particles manufacture within the size range of 60–100 µm and with spherical morphology (Figure S1 and

S2). Such sizes are significantly larger than those of malignant cells, allowing for adhesion of multiple cells to MPs, and the establishment of cell-cell interactions that are crucial for 3D aggregates self-assembly [49]. Following this preliminary size optimization, MPs were sieved and the percentage of particles in the desired size significantly increased from 49.5%, up to 95.2%. With this approach, the final MPs formulations exhibited a mean size of 83 μm and a relatively small coefficient of variation (CV:14.86%) (Fig. 2B).

For PCL MPs surface functionalization with HyA ECM-mimetic coatings, the formulations were initially subjected to plasma treatment to increase hydrophilicity and promote a more efficient layer-by-layer (LbL) deposition of positively charged Poly-L-lysine (PLL) onto PCL particles surface. HyA was chosen to functionalize MPs outermost layer since this is a key component of human tumors-ECM, being generally associated to poor disease prognosis in patients with lung cancer [17,51]. Different reports in the literature support the use of PLL/HyA LbL layered particles for promoting embryonic stem cells adhesion/proliferation in 3D culture [52].

To study the surface deposition of polyelectrolyte polymer nanolayers and sequential surface charge reversal, zeta potential measurements where performed. The obtained negative zeta potential was in accordance with the charge of the HyA outermost polymer layer deposited onto MPs surface (Fig. 2C). Despite PLL/HyA 2 bilayers build up present negative zeta potential these films could be highly irregular. Hence, a coating of PLL/HyA 3 bilayers was selected to assure higher film homogeneity, whilst providing a rough surface for cells adhesion. Following LbL surface functionalization, PCL particles maintained both their size distribution, and morphology (Fig. 2, D1-3), with only a minor increase on surface roughness being observed (Fig. 2, D4-6). Furthermore, particles subjected to LbL functionalization with 3 bilayers of PLL/HyA showed no tendency to aggregate when incubated in culture medium (Supplementary Figure S3). Therefore, following the successful optimization of the LbL process for the obtention of bioinstructive microparticles coated with HyA, different assays were performed to access how the inclusion of LbL-MPs promoted 3D spheroids self-assembly and tumor mimicking features during *in vitro* culture.

3.2. 3D-MCTS assembly and morphological characterization

Culturing cells *in vitro* in a 3D setting, rather than in flat 2D substrates, provides the representation of key solid tumors hallmarks such as the formation of a necrotic core and the recapitulation of cell-cell tridimensional physical interactions and intercellular crosstalk [47,53–55]. With the objective of mimicking such characteristics, microparticle-based tri-coculture 3D tumor models containing non-small cell lung cancer cells (A549), human dermal fibroblasts (HF), and bone-marrow derived human mesenchymal stem cells (hBM-MSCs), were established by using disease relevant cell-cell ratios based on previous literature reports [30,36–38,41,42].

Prior to assembly of these complex models, a preliminary optimization of spheroid cultures involving mono and dual co-culture spheroids of A549: HF assembled with different cell numbers (e.g., 5, 10, 15, 30 and 45 000 cells) and varying amounts of LbL-MPs (e.g., 0.025 or 0.050 mg/well) was investigated. Image analysis over time allowed to access 3D microtumor growth and circularity/compaction (Figure S4, S5 and S6). Such variations in cell seeding densities and microparticle combinations were explored to establish 3D-MCTS with sizes capable of exhibiting nutrient, metabolite and hypoxic gradients (e.g., size > 500 μm) [56]. Establishing a necrotic core in the interior of the spheroid, while maintaining solidity and shape uniformity over extended periods of culture is important to reduce assay-to-assay variability.

The obtained results demonstrate that A549 monocultured spheroids have the widest areas, lowest circularity and compactness, indicating the formation of relatively uncondensed 3D agglomerates at day 1. Such was clearly visible in optical contrast micrographs obtained for the various 3D spheroids formulations as shown in Figure S4. Interestingly, over the period of 14 days, A549 monoculture spheroids had a gradual process of aggregation, becoming a compact and circular 3D microtissue (Figure S4A). The addition of LbL-MPs to A549 cells promoted an aggregation alike that of 3D spheroids formed only by a continuous cell mass. Such indicates that HyA-coated MPs offer a suitable cell-anchoring scaffold for cancer cells to attach and assemble into a spherically structured microtumor mass *in vitro* (Figure S4B and C).

Following the successful assembly of spherically structured LbL-MPs homotypic models, 3D spheroids formed by A549:HF dual co-cultures were established so as to better represent the cancer-stroma microenvironment of human tumors. The addition of dermal fibroblasts in A549:HF 1:2 ratio, lead to the formation of significantly smaller and more circular microtumors (Figure S5A and B), when compared to their monotypic counterparts. A similar result was obtained with A549:hBM-MSCs dual coculture spheroids (Figure S6A and B). Interestingly, the 3D microtumors containing HF or hBM-MSCs already exhibited highly compact morphologies at day one, suggesting that cancer cells close interactions with mesenchymal stem cell populations play a major role in shaping the tumor mass and microenvironment (Figure S5 and S6). These findings are in accordance with those reported by Dittmer and coworkers [57], for breast cancer cells and hBM-MSCs co-cultures, and emphasize the importance of not only including supporting fibroblasts, but also mesenchymal stem cell stromal populations in tumor models. To the best of our knowledge this is the first time a tri-coculture of these cells is investigated in an *in vitro* 3D setting. During this optimization we investigated the effect of MPs amount in 3D models' assembly kinetics and final morphology/compactness. As the results demonstrated, the addition of either 0.025 or 0.050 mg of LbL-MPs per cell culture well in the ultra-low adhesion plates, resulted in slightly higher spheroid areas at initial time points, in comparison to control, particle-free 3D spheroids (Figure S4, S5 and S6). More importantly, the cells successfully adhered and proliferated in contact with hyaluronic acid functionalized MPs along time, with functionalized MPs fulfilling their ECM-mimetic function (Figure S4, S5 and S6).

The addition of 0.025 mg LbL-MPs to each well demonstrated the best results regarding spherical shape and reproducibility. It is important to emphasize that, in preliminary assays, spheroids with low cell density (5000 cells), and containing 0.050 mg of microparticles were unable to form cohesive spherical microtissues.

After establishing the optimal culturing conditions for A549 and A549:HF spheroids, the formation of tri-coculture spheroids at a ratio of 10:20:1 (A549:HF:hBM-MSCs) was investigated. The ratio of cancer cells to hBM-MSCs was selected from a previous report by Liu and coworkers, which discovered that smaller ratios of MSCs to A549 cells seem to favor pro-tumorigenic interactions *in vitro* [30]. This low ratio is also representative of what occurs in human tumors, since only a limited number of MSCs migrate from the bone marrow to the tumor mass *in vivo* [34].

Spheroids circularity and area analysis in the conditions where A549 cells were combined with hBM-MSCs, revealed that tri-coculture spheroids had the smallest sizes and formed the most densely packed microtissues of all conditions including those comprising HyA MPs, as shown in Fig. 3.

3.3. 3D-MCTS cellular viability and necrotic core formation

Analysis of mono, dual and tri-coculture 3D tumor microtissues, assembled by cells self-aggregation or guided by LbL-MPs anchoring platforms, demonstrated that sizes higher than 500 μm were easily obtained, indicating that the followed methodology is suitable to obtain large tumor spheres. As mentioned, in this size range, cells are subjected to nutrient/oxygen/pH gradients and generally start to form a characteristic necrotic core similar to that obtained in human solid tumors [58]. To analyze if a dense mass of necrotic cells was formed Live/Dead assays based on spheroids staining with Calcein-AM (Cal-

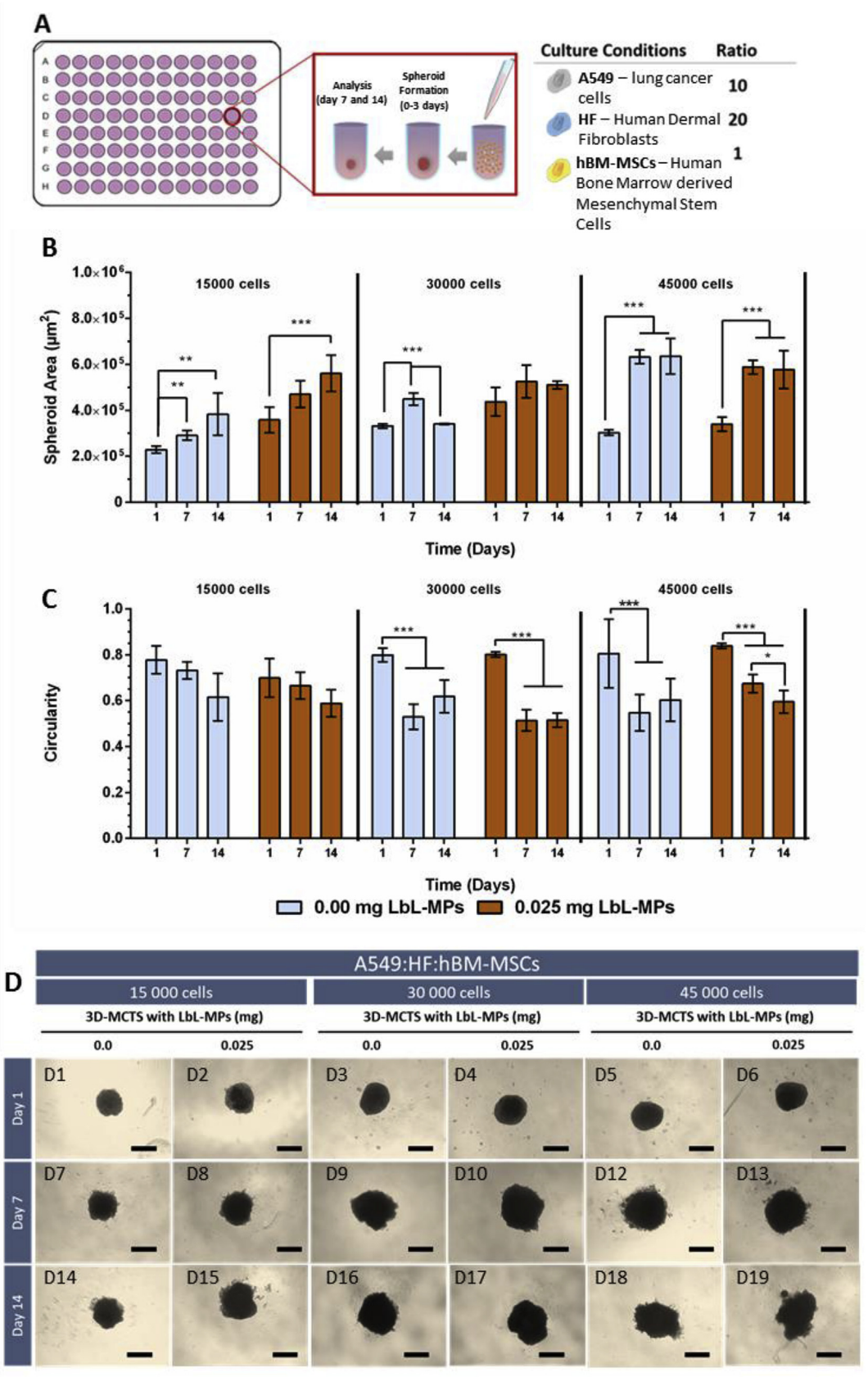

Fig. 3. 3D microtumors formed by Tri-coculture of A549:HF:hBM-MSCs and their evolution from 1 to 14 days of culture. (A) Schematics of 3D tri-coculture models established in 96 well ultra-low adhesion plates, at specific cancer-stromal cells ratios. (B) Spheroids area quantification, and (C) quantitative circularity measurements (1 = perfect circle, 0 = line) were performed by using image Analyze/Measure algorithms contained in ImageJ v.1.8.0. (D) 3D microtumors morphological analysis by optical contrast microscopy. Scale bar represents 500 μm.

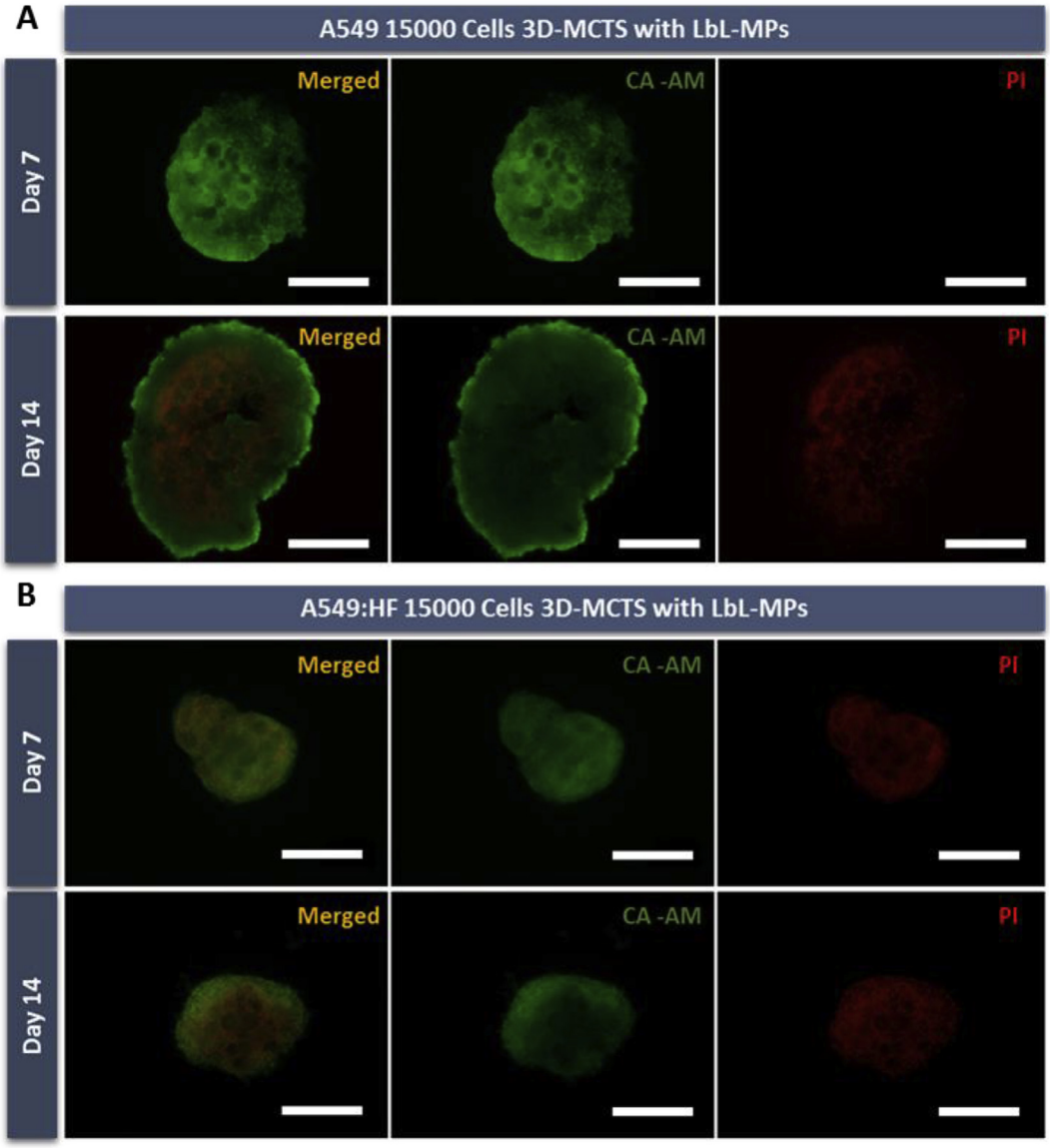

Fig. 4. Fluorescence microscopy micrographs of 3D-MCTS Live/Dead staining. (A) A549 single cell-type 3D spheroids and (B) dual co-culture spheroids (A549:HF), assembled in bioinstructive LbL-MPs (0.025 mg). Comparison of both conditions revealed that while in monoculture spheroids the necrotic core (red channel) was only established at 14 days of culture, in the dual coculture conditions the necrotic region was visible from day 7 onwards. Green channel: Calcein-AM, Red channel: PI. Yellow channel: merged. Scale bars = 200 μm. (For interpretation of the references to color in this figure legend, the reader is referred to the Web version of this article.)

AM)/PI were performed. As evidenced by fluorescence microscopy, in A549 MCTS containing or not LbL-MPs necrotic formation core was visible after 14 days of culture (Fig. 4 A) in models with 15×10^3 cells, but not with lower cell density (Figure S10). Interestingly, in A549:HF LbL-MPs dual coculture 3D spheroids the necrotic core was readily visible at 7 days of culture, thus evidencing that HF stromal cells promote a faster establishment of the necrotic core. Moreover, in monoculture MCTS A549 containing 30 000 cells and LbL-MPs an increased number of dead cells was visible already at day 7, with clear necrotic core formation occurring at day 14 (Supplementary Figure S13). This indicates that LbL-MPs inclusion further approached these models to those obtained through co-culture with either HF or hBM-MSCs, possibly by physically decreasing penetration of nutrients and oxygen into the inner spheroid regions, or\and through HyA derived upregulation of adhesion mechanisms, as evidenced by CD44 upregulation (Fig. 9). Moreover, in all tested conditions the established necrotic core was also denser at 14 days, an important feature that influences the penetration of nutrients/oxygen into deep microtumors regions [59,60].

Live/dead analysis of tumor-mimicking tri-coculture (A549:HF:hBM-MSCs) 3D spheroids with and without LbL-MPs, also revealed the establishment of well-defined necrotic regions at 7 days (Fig. 5, A), for all conditions (15 000 to 45 000 initial cells, Fig. 5). Moreover, the characteristic cell-proliferative rim at spheroids outer region was readily visualized in both conditions (Fig. 5A and B) Interestingly, despite literature reports describing breast cancer 3D spheroids disruption and loss of stability upon MSCs addition [61], in the lung cancer 3D models produced with cells alone, or with HyA MPs, no changes were observed during the 14 days of culture. Instead, in A549:HF:hBM-MSCs 3D spheroids, a constant density and spherical morphology was observed from day 1 onwards (Figs. 3 and 5). This indicates the importance of hBM-MCSs inclusion in different tumor models since they may trigger differential responses.

The obtained results regarding the establishment of the necrotic core and the characteristic proliferative rim (Fig. 5) indicate that the produced 3D spheroids recapitulate these two major aspects of *in vivo* solid tumors. These are extremely important hallmarks of solid human

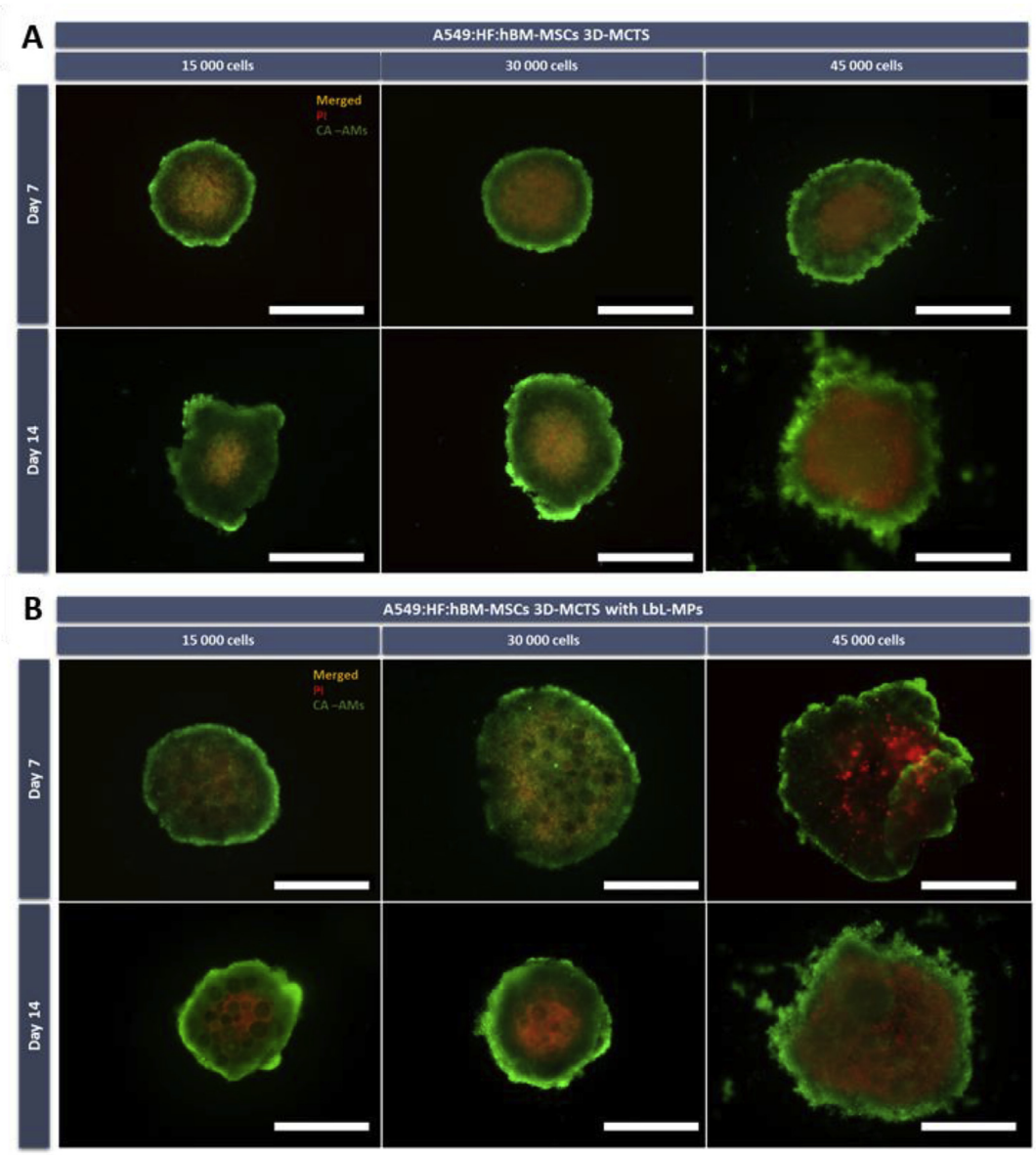

Fig. 5. Fluorescence microscopy micrographs of tri-coculture 3D-MCTS Live/Dead staining. These assays were performed in tri-cocultured A549:HF:hBM-MSCs 3D spheroids and the samples were analyzed by widefield fluorescence microscopy at 7 and 14 days post seeding, revealing necrotic core (red channel) formation in all cell seeding conditions for tri-coculture spheroids, containing (B), or not (A) functionalized LbL-MPs. Green channel: Calcein-AM, Red channel: PI. Yellow channel: merged. Scale bars = 500 μm. (For interpretation of the references to color in this figure legend, the reader is referred to the Web version of this article.)

tumors, and their recapitulation shows the potential of the assembled LbL-MPs 3D tri-coculture tumor models. Interestingly mimicking the growth kinetics with cultured cells in a tumor-like microenvironment promotes the establishment of metabolical and phenotypical cell traits [55,62,63]. Adding to this, the accumulation of catabolites and growth factors such as VEGF or HIF-1α, decurrent from increased hypoxic conditions and associated cellular dead can lead to phenotypic alterations in cancer cells and associated MSCs [64]. Such could give rise to pro-tumoral interactions between MSCs and cancer cells as described by Chaturvedi and coworkers, for breast cancer and BM-MSCs co-cultures, in which a hypoxic environment promoted metastasis [65]. The, accumulation of hypoxic and pro-inflammatory factors can also lead to an increased propensity for metastasis and multi drug resistance. These are critical aspects that should be considered when using these 3D microtissues as drug screening platforms [10,55]. To complement live/dead assays and to study whether the insertion of LbL-MPs into cultures elicited a cytotoxic effect, cell viability assays were performed in microtumor models by using Alamar blue (Figure S7, S8 and S9). Viability assays performed in the tested culture conditions showed that the inclusion of bioinstructive LbL-MPs for assembly of microtumors had no effect in cells metabolic activity. Also, the obtained results demonstrated that independently of LbL-MPs amount, no statistically significant variation in cell viability was observable when comparing LbL-MPs spheroids to standard, cell only, 3D-MCTS, both at 7 and 14 days of culture.

Taking into consideration the former results regarding area, circularity, compactness, necrotic core formation and metabolic activity over time, 3D spheroids formed with and initial number of 30 000 cells were selected for subsequent studies. The area and morphology of these spheroids was then characterized in a larger scale as portrayed below, through the analysis of $n = 30$ spheroids for each condition, to assure a high confidence level for the envisioned drug screening studies.

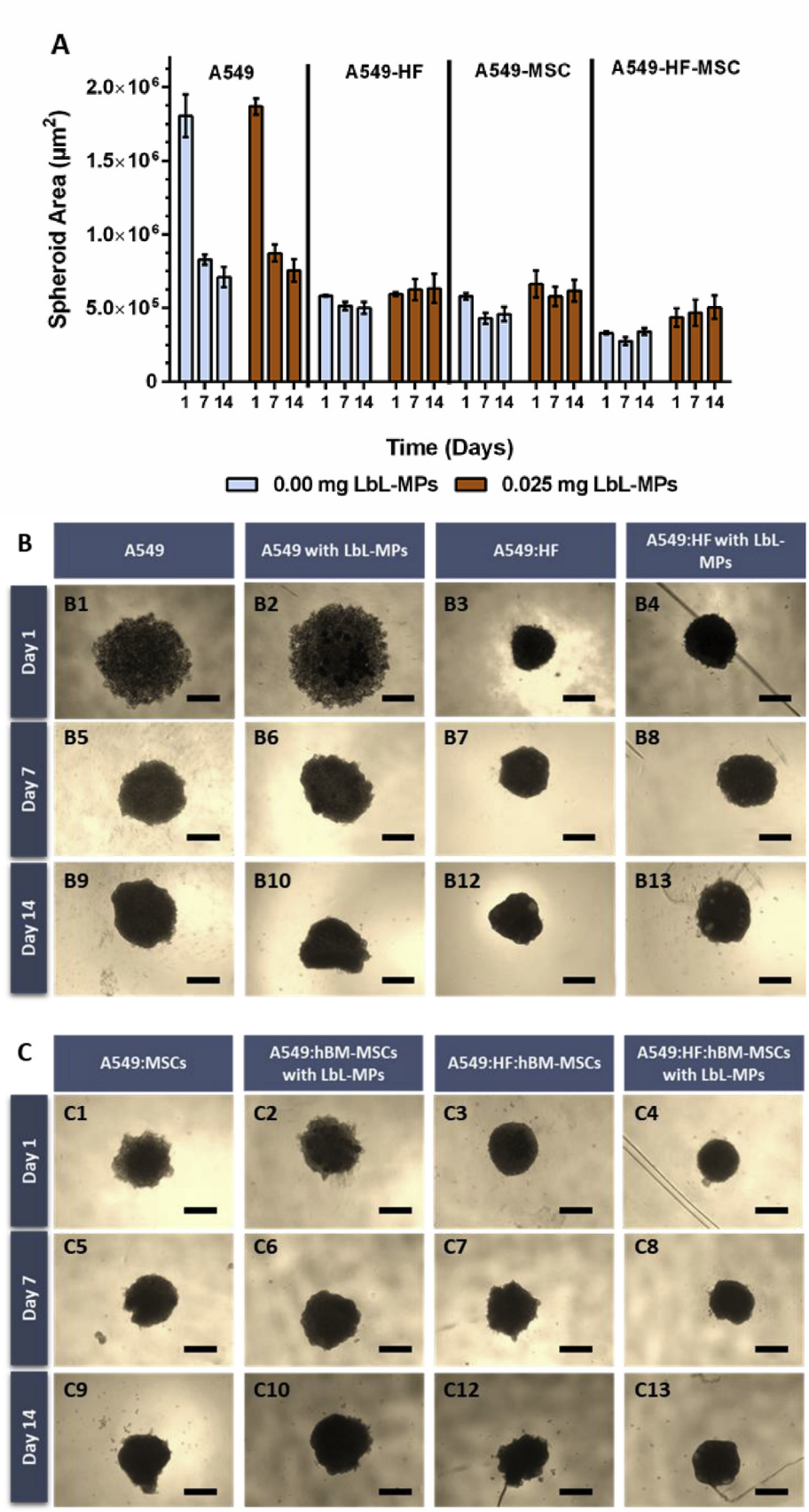

Fig. 6. Size variation of heterotypic 3D spheroids over time. (A) Area analysis of 3D-MCTS formed with 30 000 cells and assembled with different cell populations. (B and C) Optical contrast micrographs of 3D spheroids morphology obtained at different time points (1, 7 and 14 days post seeding). Scale Bars = 500 µm.

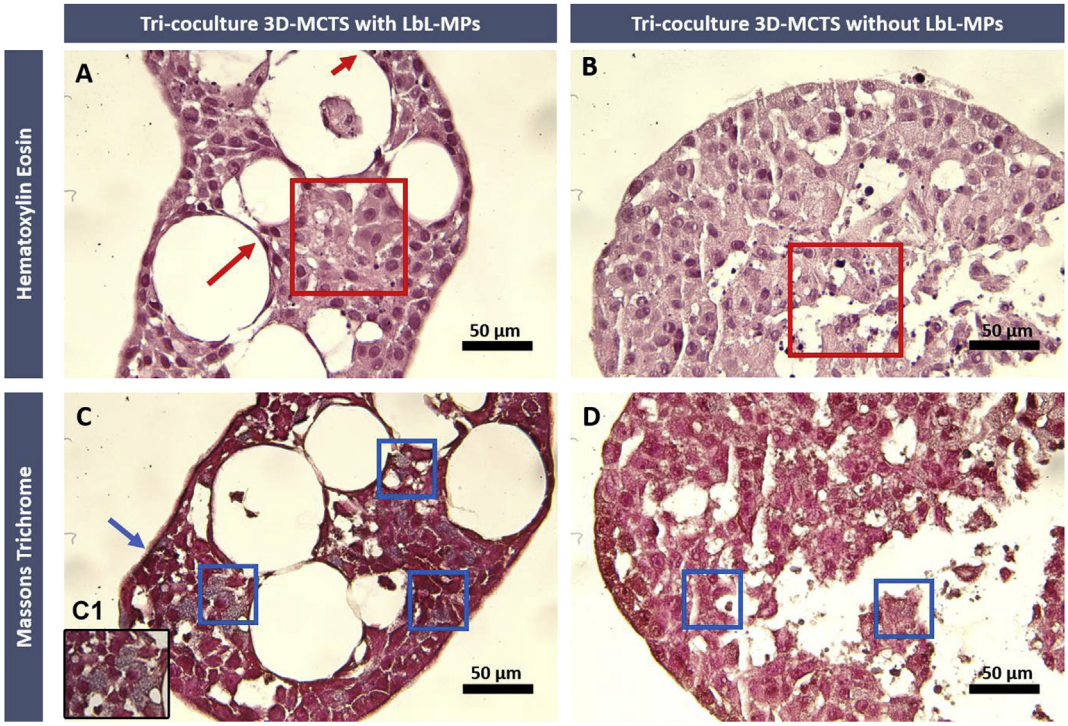

Fig. 7. Histological analysis of A549:HF:hBM-MSCs tri-coculture spheroids. (A and B) Spheroids with and without LbL-MPs. (C and D) Internal organization of cells around MPs. Image A, with cells clearly adhering to the surface of LbL-MPs and acquiring an elongated shape (A – red arrows), furthermore a possible necrotic region is observed (red circle). (C and D) At day 7 ECM deposition is already visible in both spheroids occurring however more markedly in tri-coculture 3D spheroids with LbL-MPs (C1 and blue arrow). Scale bar = 50 µm. (For interpretation of the references to color in this figure legend, the reader is referred to the Web version of this article.)

In comparison to monocultured models, dual cocultures and tri-coculture 3D-MCTS with and without LbL-MPs, presented increased contraction (Fig. 6). This observation could be related to ECM components secretion mediated by HF and MSCs, since these two cell types are recognized to contribute immensely to ECM deposition in human TME [39].

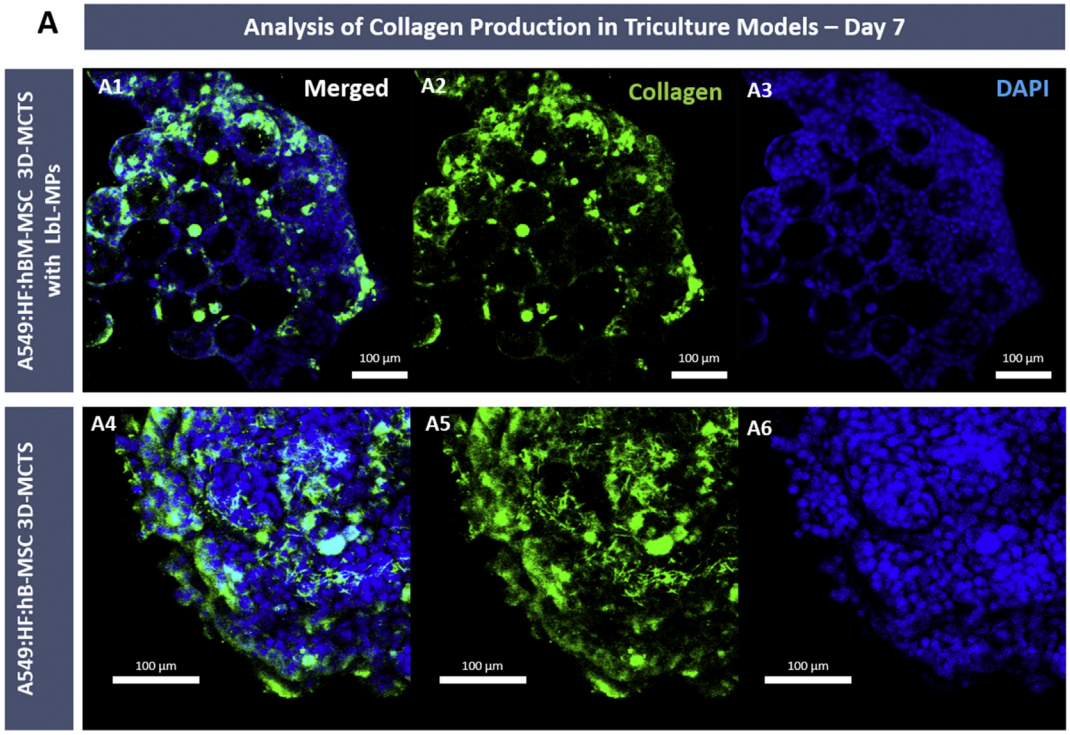

Fig. 8. CLSM micrographs of tri-coculture spheroids at 7 days of culture. (A) 3D spheroids assembled with and without bioinstructive HyA MPs presented collagen deposition. Green channel: anti-collagen type I-FITC conjugate antibody. Blue channel: DAPI nuclear staining. Scale bars represent 100 µm. (For interpretation of the references to color in this figure legend, the reader is referred to the Web version of this article.)

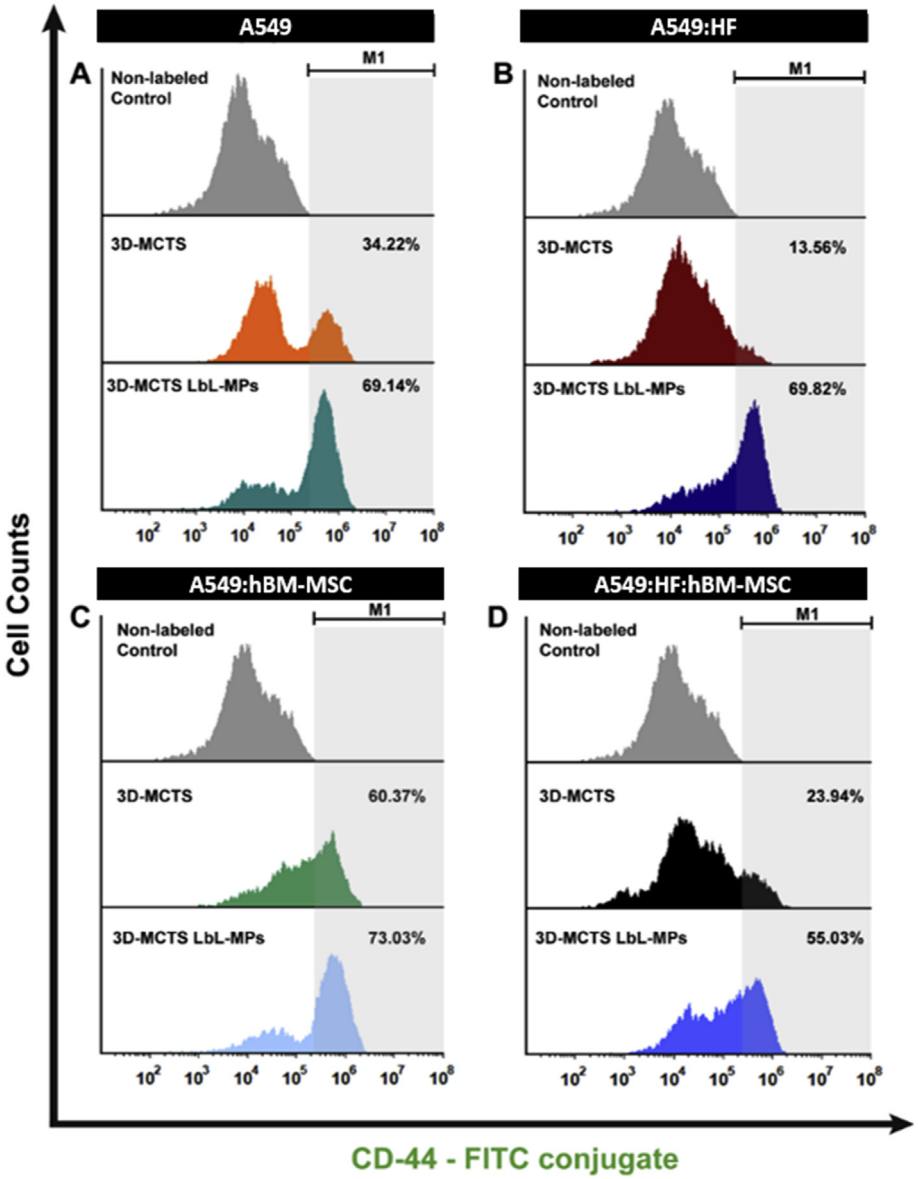

Fig. 9. Flow cytometry analysis of CD44 surface marker expression in various 3D tumor spheroids at 7 days of culture. M1 – marker represents the gated ROI for analysis. 3D-MCTS - represents 3D spheroids formed only by cell-cell aggregates without LbL-MPs. Addition of LbL-MPs to spheroids contributed for a visible increase in CD-44 expression.

3.4. 3D-MCTS histological analysis

H&E and Masson's Trichrome (MT) staining were performed in A549:HF:MSCs 3D spheroids histological sections to evaluate microtumors deep internal organization when cultured with LbL-MPs and to investigate ECM components deposition (e.g., collagen) within the spheroids mass. The histological analysis of 3D microtumors sections, revealed a compact internal cellular organization similar to that of solid human tumors. Compared to other reports with A549 spheroids this result seems to be expected for the established culture times [66]. A closer analysis of spheroids containing LbL-MPs revealed that cells adhering to microparticles were completely spread and extended over their surface, thus establishing contact on one side with the HyA matrix and on the other with surrounding cells (Fig. 7 A, B). Furthermore, regions with LbL-MPs presented a clearly delimited and spherical void space (Fig. 7 A and C).

Regarding tri-coculture spheroids, Masson's Trichrome (MT) staining that at day 7 showed that collagen deposition in microtumors core containing LbL-MPs is starting to be detected (Blue stained regions Fig. 7C and D). This result is in accordance with the increased contraction rates observed in tri -coculture spheroids when compared to its A549 monoculture counterparts. To further complement collagen deposition, immunofluorescence labeling of collagen I in whole 3D spheroids mass was performed.

3.5. Immunocytochemistry analysis of 3D-MCTS ECM components

Collagen I immunocytochemistry analysis was also performed in A549-HF-MCSs 3D spheroids to further analyze collagen deposition and if the increased cohesion observed by optical microscopy analysis of tri-coculture models could be associated with the deposition of tumor-ECM components. Collagen is an abundant structural component of the human ECM, is constituted by several diverse types of which collage type I is the predominant form in most tissues [67]. During tumor progression established interactions between fibroblasts and cancer cells can lead for example to increased matrix deposition and collagen cross-linking, resulting in changes in ECM architecture [67]. This is characterized in part by increased collagen re-deposition/crosslinking,

and ultimately leads to matrix stiffening. From a therapeutic perspective this event strongly contributes for the establishment of a barrier to chemotherapeutics penetration and hinders their efficacy in deep tumor regions [68]. While the role of collagen in the TME has not yet been fully elucidated [67], increased collagen deposition in 3D spheroids has been linked with increased interstitial pressure. Moreover, an increased collagen deposition has also been connected with an increased metastatic potential in breast cancer [69].

The results obtained by immunocytochemistry revealed that at day 7, collagen deposition was clearly visible in LbL-MPs 3D tri-coculture microtumors mass (Fig. 8). Such leads to the formation of a network of collagen fibrils over the 3D spheroid volume and can contribute to spheroids cohesion and the establishment of a necrotic core. Moreover, collagen deposition and fibril alignment are recognized as key factors involved in cancer cell invasion of tissues resulting of microenvironment remodeling by cancer cells, being associated with the development of pro-metastatic cell phenotypes in breast, lung and prostate cancer [69–71].

Overall these findings demonstrate 3D spheroids ability to closely mimic key solid tumor features through *de novo* collagen deposition. It is important to emphasize that the produced collagenous matrix can act both as a structural component and as a store house of cellular signaling factors (e.g., growth factors) [72] during *in vitro* culture. Following this *de novo* tumor-ECM characterization, we aimed to investigate the role of LbL-MPs inclusion in the overexpression of key cancer cells surface markers, in particular, the cluster of differentiation 44 (CD44), which is widely recognized by its ability to interact with ECM hyaluronan.

3.6. Flow cytometry analysis of CD44

Several studies reported that in contact with hyaluronic acid-rich substrates, cancer cells increase their expression of the CD44 cell surface receptor [72,73]. Increased CD44 expression has been intimately connected with cancer multi-drug resistance (MDR) and with the development of cancer stem cell-like phenotypes [74,75]. As such, the effect bioinstructive LbL-MPs on CD44 cell surface receptor expression in mono-, dual and tri-coculture 3D microtumors was evaluated (Fig. 9).

The obtained results show a clear increase in CD44 expression in mono-, dual and tri-coculture 3D spheroids upon the inclusion of bioinstructive LbL-MPs emphasizing their importance as tumor mimicking *in vitro* platform. In particular, dual cocultures of A549: HF and tri-cocultures experienced approximately a ~2 fold increase in the percentage of $CD44^+$ cells when adhered to LbL-MPs *in vitro*. Interestingly, dual cocultures of A549:hBM-MSCs inherently express high levels of $CD44^+$ cells. Taking into consideration the A549:hBM-MSCs, 1:10 ratio, this high expression of CD44 can be related both with the inclusion of $CD44^+$ hBM-MSCs [31], and can also be attributed to the interactions established between cancer-MSCs populations, which lead to this increase as widely reported in the literature [73,76,77]. Overall, from a cancer biology perspective an increase in CD44 during tumor development is an observed event that is herein recapitulated with the inclusion of LbL-MPs. These findings corroborate the bioinstructive role of LbL-MPs in 3D-MCTS, evidencing their ability to act as an ECM mimetic support, in this case via HyA. It is important to emphasize that due to LbL technique versatility PCL microparticles may be functionalized with additional tumor-ECM components in the future.

Having established the validity of using bioinstructive LbL-MPs to obtain relevant 3D *in vitro* tumor models we then evaluate the migration/role of hBM-MSCs in the formed microtumors since to the best of our knowledge this is the first time a tri-coculture of A549:HF:hBM-MSCs has been established *in vitro*. Hence, considering the growingly recognized role of tumor infiltrating MSCs we characterized the trafficking of MSCs when included in the 3D microtumors mass.

3.7. Tri-coculture 3D spheroids cells tracking and migration overtime

As emphasized, previous reports demonstrated that hBM-MSCs display an intrinsic ability to migrate and deeply penetrate into tumor masses [78,79]. As such, time-course cell tracking assays were performed with the aim of better understanding the internal organization of tri-coculture spheroids, and to observe if hBM-MCS posteriorly added to already formed tumor spheroids present dynamic migration patterns and exhibit a preferential location in tumor microtissues. For this purpose, all cells were stained, at the moment of tri-coculture formation, with long-term cell tracking lipophilic dyes [80], A549, (DiO - green), HF (DiL - yellow), and hBM-MSCs (DiD - red) (Fig. 10). These staining agents were transferred through subsequent cellular generations, with no considerable signal loss being observed up to 14 days of culture, after which the intensity of the staining started to fade. Such approach allowed a qualitative assessment of the localization and migration of different cell populations in the spheroid structure over time. Alternatively, hBM-MSCs stained with DiD were subsequently added to spheroids at day 7 of culture, to access hBM-MSCs ability to migrate and penetrate the produced tumoral 3D microtissues comprised by different cell populations.

The obtained results, regarding tri-coculture spheroids, demonstrate that over the course of 7 days, cultured hBM-MSCs have a tendency to migrate to and localize in deep internal regions of tri-coculture spheroids. Furthermore, fluorescence microscopy data also confirmed that cultured cells seem to adapt to LbL-MPS morphology (Fig. 10), extending themselves over the exposed surfaces as observed in histological analysis (Fig. 7).

Furthermore, over the course of 14 days, the fluorescence signal emitted by DiD (the cell marker associated hBM-MSCs), was clearly visible, denoting the presence of MSCs. The obtained high-resolution micrographs also demonstrate an internal organization of mesenchymal stem cells into hotspots inside tri-coculture spheroids. These clusters are surrounded by numerous A549 cancer cells and dermal fibroblasts with no apparent well-defined spatial organization (Fig. 11, at 14 days). Moreover, as shown in Fig. 11A and B, in both cell-cell agglomerated or LbL-MPs structured tri-coculture 3D models, MSCs demonstrated a tendency to condense into MSCs rich agglomerates along time. Interestingly, at early time points (3 and 7 days), hBM-MCSs are still randomly dispersed in LbL-MPs 3D microtumors (Fig. 11, B4 and B8). Yet, at 14 days of culture, a clear stem cells agglomerate was observed in 3D spheroids center (Fig. 11, B12).

These interesting findings led us to evaluate MSCs migration into 3D tumor models also after their formation, as this would better recapitulate the *in vivo* scenario of stem cells tropism to tumor sites [34,81]. Cell tracking analysis clearly showed that upon addition of DiD-stained hBM-MSCs to pre-formed 3D spheroids, these cells were able to migrate to the interior of mono and coculture microtumor masses in all tested conditions, after only 24 h of incubation (Fig. 12). Furthermore, it is interesting to denote that despite hBM-MSCs presence in dual-coculture and tri-coculture models, the administered hBM-MSCs still adhered, penetrated and migrated in these spheroids. In all the conditions tested, hBM-MCS organized into clusters in the microtumors mass (Fig. 12A and B,C,D at 168 h), providing important evidences for further fundamental studies or therapeutic approaches [78], including such as those based on the use of MSCs as trojan horses for chemotherapeutics/nanoparticles administration to tumors [82]. To the best of our knowledge this is the first time that a tri-coculture and cell tracking analysis with hBM-MSCs has been performed *in vitro*. Such findings also emphasize that the bioengineered 3D tumor models with LbL MPs recapitulate the features of *in vivo* tumors by providing a proper niche for MSCs to settle, rearrange spatially and interact with other cells of the tumor microenvironment.

Having established the tumor-like features of A549:HF:hBM-MSCs 3D spheroids cultured in LbL-MP platforms and the successful inclusion of hBM-MSCs in the microtumor mass, the screening of a model

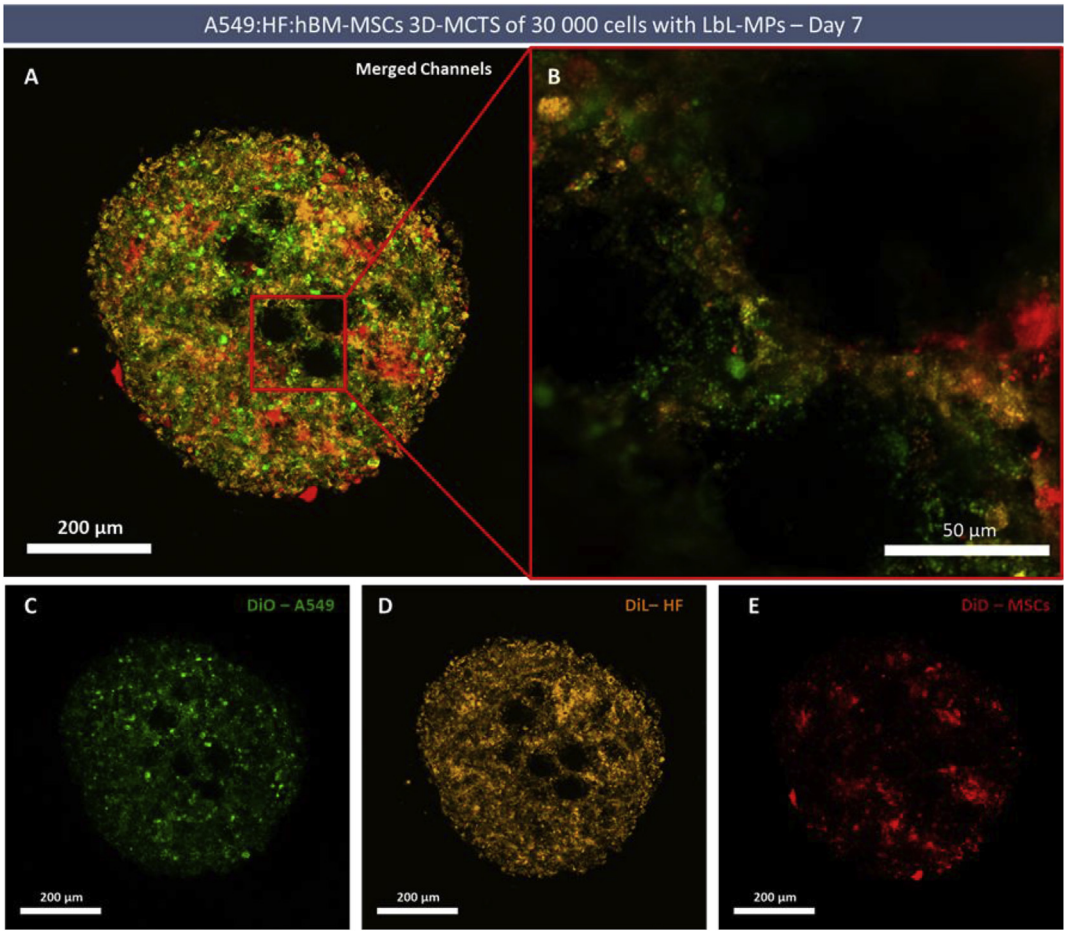

Fig. 10. High resolution CLSM confocal imaging of cellular organization in tri-coculture LbL-MPs spheroids at day 7. (A) CLSM micrograph with merged channels. (B) Magnified section containing cells attached to LbL-MPs. (C) DiO labelled A549 cancer cells – green channel. (D) DiL labelled fibroblasts - yellow channel. (E) DiD labelled MSCs – red channel. Mesenchymal stem cells acquire a cluster-like arrangement. (For interpretation of the references to color in this figure legend, the reader is referred to the Web version of this article.)

chemotherapeutic compound (Doxorubicin) cytotoxic activity in these models was then investigated with the aim to draw relevant conclusions regarding the influence of hBM-MSCs and LbL-MPs inclusion in 3D *in vitro* lung tumor models.

3.8. Chemotherapeutics drug screening in bioinstructed 3D-MCTS

Interactions between diverse populations present in the TME are known to be of paramount importance for the performance of chemotherapeutics. In fact the close interactions established between stromal and cancer cells through direct contact or indirect soluble cues such as cytokines, chemokines and growth factors ultimately lead to altered metabolic profiles, signaling pathways, and invasive behavior [83]. Moreover, this communication incites drug resistance through several cancer cells defense mechanisms that include a decreased uptake of water soluble chemotherapeutic compounds, and the modification of cancer cells metabolic regulation either through 'self-genetic' mutation or interaction with cellular components of the tumor microenvironment (TME) (e.g., fibroblasts, immune system cells and MSCs). Such unique crosstalk between cancer cells and their TME may lead to a decreased cell cycle arrest, increased repair of DNA damage, reduced apoptosis, and an increase in energy-dependent efflux of hydrophobic chemotherapeutics such as Doxorubicin is also often obtained [84,85]. The result is an area were therapeutic agents' penetration is possibly hindered. From a bioengineering point of view, modeling these hallmarks of *in vivo* tumors within 3D *in vitro* tumor models is highly desirable.

The coculture of cancer cells with HF and hBM-MSCs and the existence of a necrotic core signalizes the lack of nutrient and medium penetration into 3D microtumors deepest regions. By establishing a 3D coculture model capable of representing *in vitro* A549 cancer cells *in vivo* like interactions with HF and hBM-MSCs, we aimed to recapitulate tumor cellular heterogeneity [40,42,78,86]. Furthermore, the inclusion of hyaluronan aimed to recapitulate tumor-ECM components. In fact, in lung cancer TME, HyA is associated with poor tumor cell differentiation and higher recurrence rate when present in elevated quantities [17]. Moreover, interactions of LbL-MPs with stromal cells such as HF or MSCs, have also been connected as possible roots towards establishment drug resistance phenotypes [20].

Drug screening assays were then performed to access the influence of HyA and heterotypic tri-cocultures in comparison to more simplistic 3D *in vitro* tumor models formed only by cancer cells or by non-functionalized MPs. For this purpose, Doxorubicin (Dox) was administered to 3D spheroids cultivated over a period of 7 days, to allow the establishment of cell-HyA and cell-cell contacts. The inclusion of LbL-MPs into 3D spheroids generally originated a slightly higher cell viability when compared to control 3D microtumors or NT-MPs spheroids (Fig. 13A–C). The obtained higher viability in tri-coculture with HyA MPs was more pronounced in A549 monotypic spheroids ($^*p < 0.05$). The lack of a significant increase in resistance in dual and tri-coculture LbL-MPs spheroids could be correlated with the inclusion of stromal cells and added models' complexity. Importantly, non-functionalized PCL MPs (NT-MPs) exhibited a higher susceptibility to Dox in comparison to tri-coculture 3D spheroids (Fig. 13A–D, 3D-MCTS with NT-

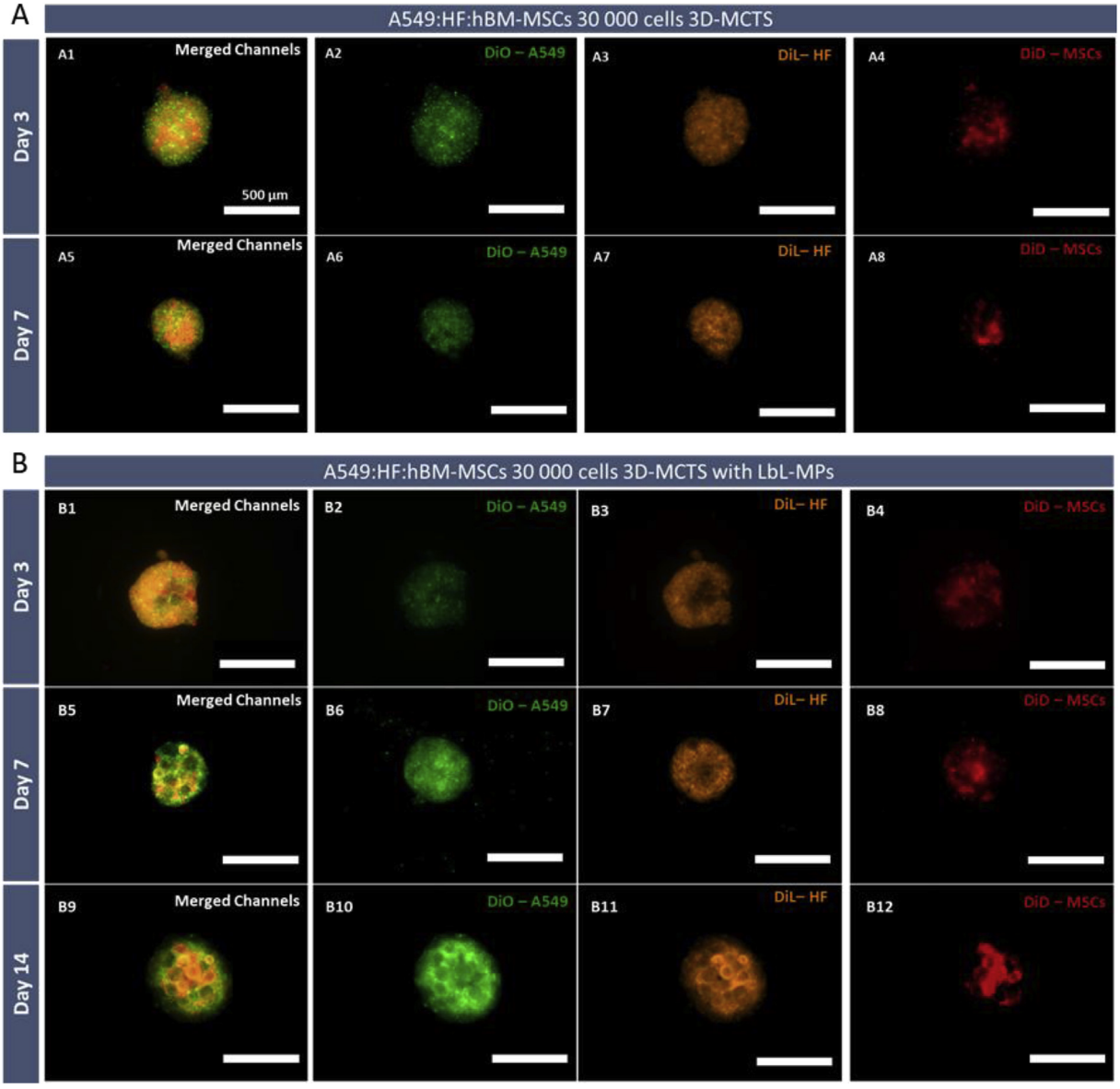

Fig. 11. Widefield fluorescence micrographs of tri-coculture 3D spheroids stained with cell tracking dyes demonstrated a tendency in hBM-MSCs to colocalize into the interior of the spheroid. (A) Cultured hBM-MSCs formed visible cell clusters at the inner regions of the spheroids over time, taking 7 days in 3D-MCTS not containing LbL-MPs, (B) and 14 days in microtumors formed by cell agglomerates and bioinstructive LbL-MPs. Scale bar = 500 µm.

MPs), which could be associated to a lack of cellular adhesion and bioactivation, since these microparticles only present a plasma treated PCL surface and not a bioinstructive layer. These findings emphasize the successful inclusion of HyA component and its biological effects.

The acquisition of higher resistance to Dox in LbL-MPs 3D spheroids could be related to several factors, including the formation of more compact spheroids via increased matrix deposition or via increased expression of CD44 markers as demonstrated by FCM analysis. Previous works by Han and coworkers, 2016, demonstrated that A549 spheroids cells assembly was mediated through a CD44-dependent mechanism [79]. The possible establishment of cell-cell interactions between HF and A549 cells could be directly correlated with the lower Dox cytotoxicity index in these cultures, closely mimicking events in *in vivo* tumors [87].

In an overall analysis, cell-cell agglomerate 3D spheroids and LbL-MPs 3D models cultured in dual and tri-coculture, generally presented higher cell viability at the highest tested dose (17 µM Dox), than their monoculture counterparts. In addition, an all-round characterization of 3D spheroids assembled with half mass of LbL MPs (0.0125 mg) was performed (Figure S11 to S14). In summary, the obtained results demonstrate that the use of a lower mass approximated 3D LbL MPs spheroids chemotherapeutic response to that of standard 3D-MCTS, indicating that the optimized amount of LbL MPs (0.025 mg) may be a more suitable model to recapitulate the features of resistant tumors.

It is important to emphasize that these results are obtained with bone marrow derived MSCs and that MSCs of different origins may originate differential responses to chemotherapeutics as was recently reviewed [34]. Paradoxically, such interactions were found to be correlated with the establishment of pro-tumoral or anti-tumoral interactions with cancer cells. Hence, we aimed to further test this hypothesis, by establishing a non-physiological A549:hBM-MSCs ratio of 1:1, having this model been subjected to the same culture conditions and Dox concentrations. The obtained results evidence a pro-tumoral role of hBM-MSCs in A549 lung cancer cells when present in low ratios (A549:hBM-MSCs 10:1 ratio), (Fig. 14A). On the contrary, when A549 and hBM-MSCs were cultured in a 1:1 ratio a higher susceptibility to Dox was observed (Fig. 14B). Such findings demonstrate, the variable and important role of MSCs in the tumor microenvironment [30,41],

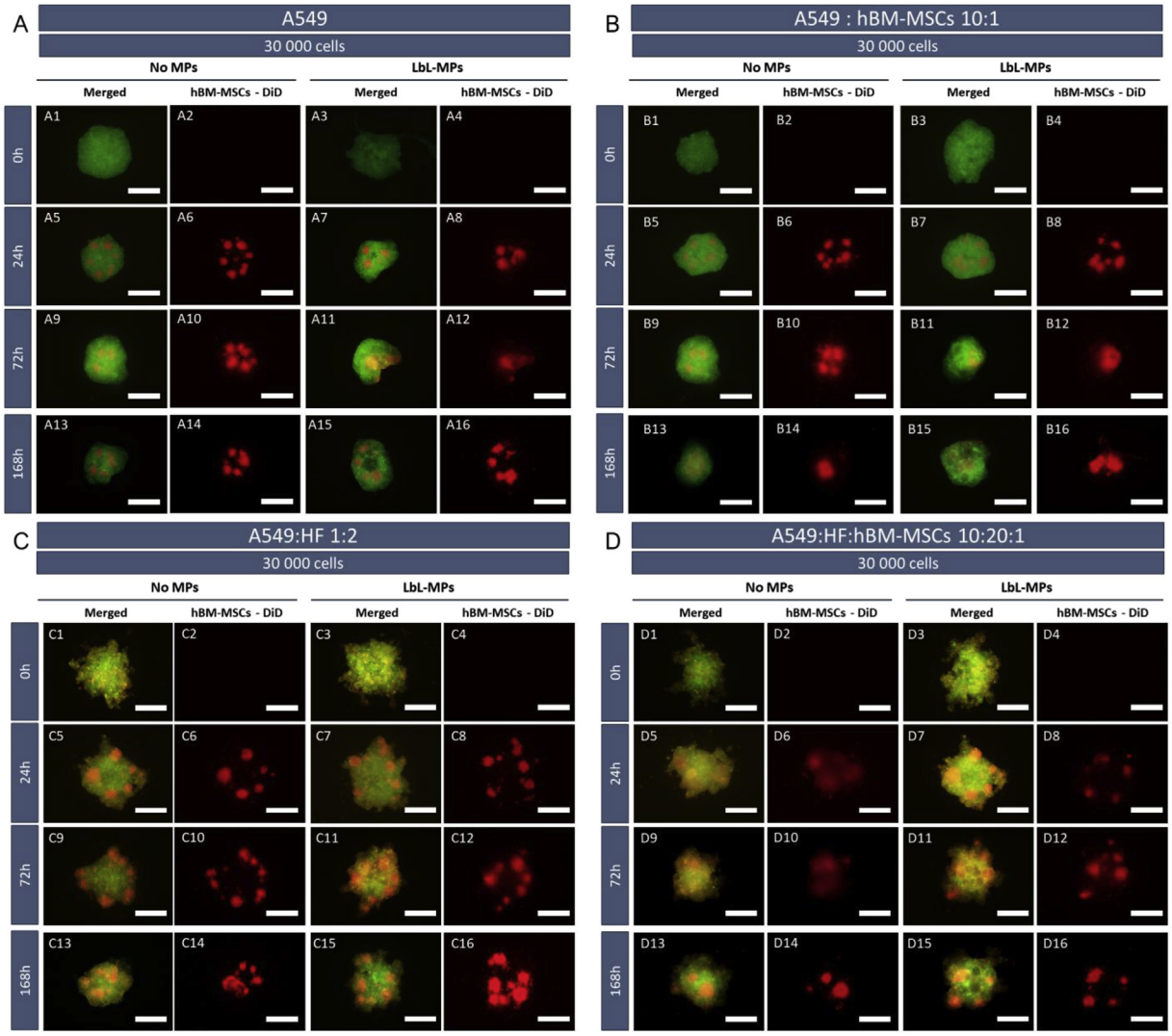

Fig. 12. Widefield fluorescence micrographs of mono (A), dual (B and C) and tri-coculture (D) 3D spheroids cells tracking. hBM-MSCs stained with DiD were added to 3D spheroids previously cultured for 7 days (t = 0 h) in ULA plates. A549 – green channel (DiO), HF – Orange channel (DiL), spheroid resident hBM-MSCs (non-labelled in condition B and D); newly administered hBM-MSCs – red channel (DiD). Scale bar = 500 μm. (For interpretation of the references to color in this figure legend, the reader is referred to the Web version of this article.)

emphasizing the importance of including this cell type in the development of *in vivo*-like preclinical drug screening platforms to achieve a more robust recapitulation of the *in vivo* tumor microenvironment.

In summary, the different data obtained through the newly established co-culture model of A549, with HF and hBM-MSCs, corroborates the necessity of further analyzing the cooperation of TME stromal cells with cancer cells in *in vitro* 3D models. It is important to mention that this was also the first time a 3D model comprising these tri-cocultures and HyA matrix in bioinstructive microparticles was developed and used as a testing platform for evaluation of chemotherapeutics anti-cancer performance, in TME relevant conditions. In the future, additional screening performed with other clinically used chemotherapeutics that have different mechanisms of cytotoxicity could further provide important insights into the employment of LbL-MPs and hBM-MSC models as *in vitro* tumor surrogates.

4. Conclusions

By taking advantage of a combination of coculture conditions, based on previous literature reports, an easy to assemble composite 3D tri-coculture model containing key TME populations such as HF and hBM-MSCs was established by using spherical microparticles as bioinstructive anchoring substrates. The inclusion of HF and MSCs stromal cells facilitated the formation of a characteristic necrotic core, the appearance of which is known to promote resistance to therapy *in vivo*. Moreover, the inclusion of bioinstructive microparticles allowed the addition of HyA, a main component of tumor-ECM that is recognized to contribute to cells response to chemotherapeutics.

Overall the inclusion of a small percentage of bone marrow derived MSCs appears to result in a positive outcome in overall microtumors cell viability, improving the ability of A549 cancer cells to form compact spheroids and resist better to Doxorubicin-induced cytotoxicity, in specific cell-cell ratios. In the foreseeable future these models may also be used for further evaluating MSCs migration, clustering, or therapeutic effectiveness as trojan horses.

In conclusion, the *in vitro* generated bioinstructed 3D-MCTS exhibit characteristics associated with *in vivo* tumors such as development of highly dense cell masses and *de novo* matrix deposition. Such hybrid 3D spheroids containing LbL-MPs served as an effective tool for tackling one of the main flaws of spheroids-based models, i.e, the integration of pre-existing ECM derived components. The assembled tri-coculture *in vitro* models can be used to screen novel therapeutic compounds for

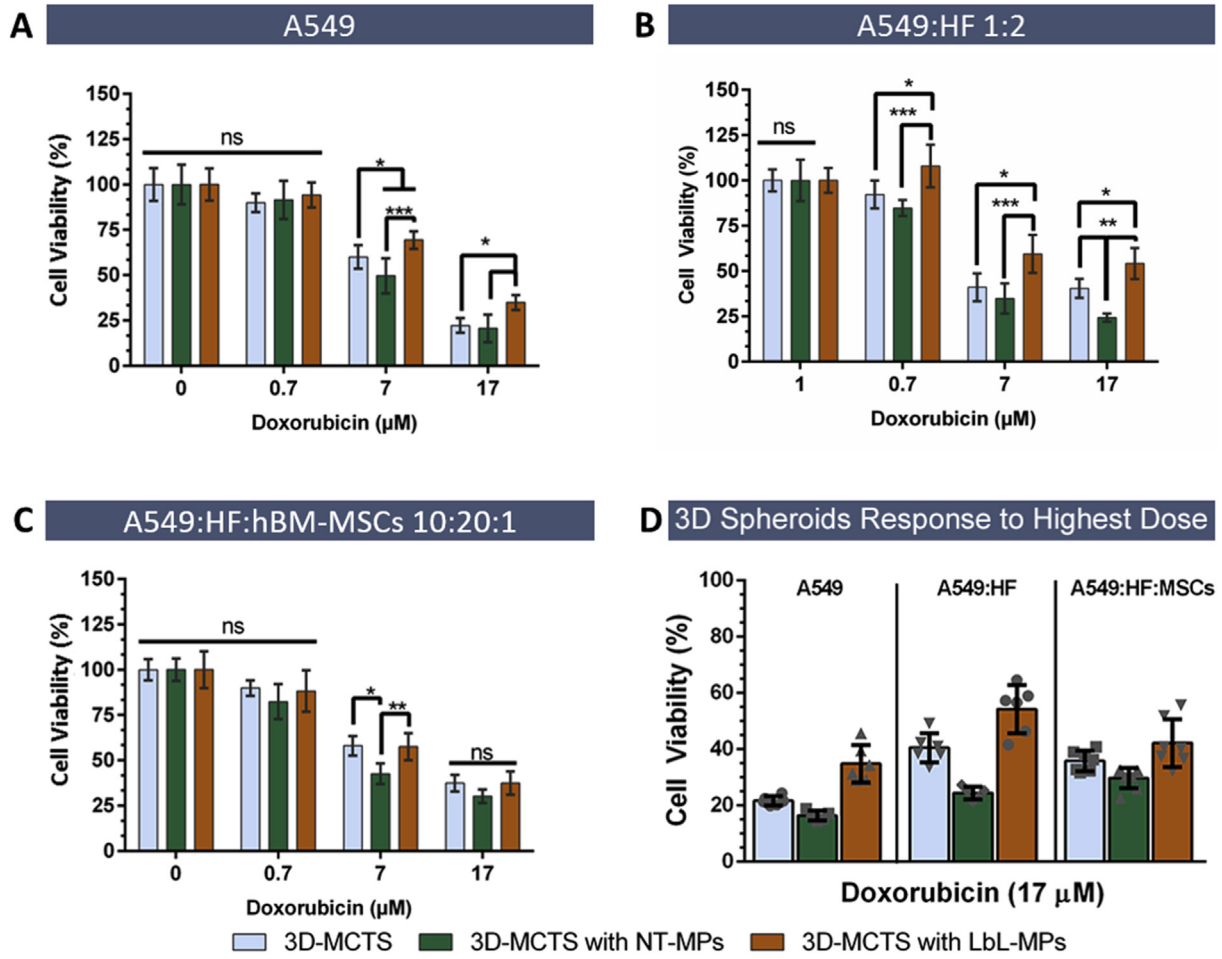

Fig. 13. Doxorubicin drug cytotoxicity screening assay performed in 3D spheroids at 7 days of culture. (A) A549 monoculture spheroids. (B) Dual coculture spheroids A549:HF. (C) tri-coculture spheroids of A549:HF:hBM-MSCs. (D) Cell viability data of all tested conditions at the highest administered dose of Doxorubicin (17 μM). Different colors represent: 3D-MCTS (control blue bars), 3D-MCTS with non-treated PCL microparticles (NT-MPs) (grey bars) and 3D-MCTS with LbL-MPs (green bars). Data is presented as mean ± s.d. (n = 6). *p < 0.05, **p < 0.01 and ***p < 0.001. ns – represents non-significant differences. (For interpretation of the references to color in this figure legend, the reader is referred to the Web version of this article.)

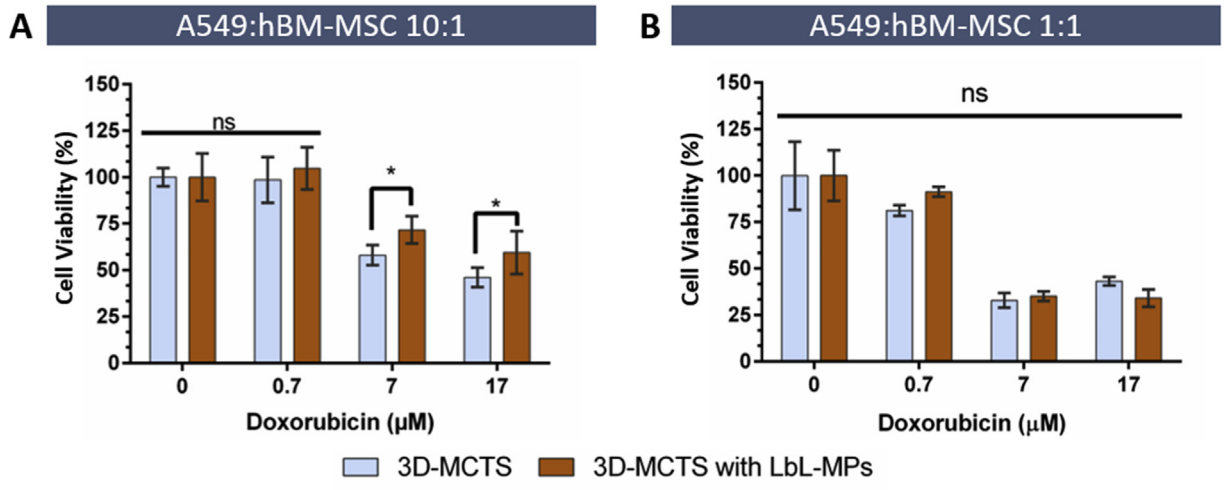

Fig. 14. Drug cytotoxicity assays of dual cocultured A549-MSCs 3D-MCTS in a 1:10 (A) and 1:1 ratio (B), respectively. Data is presented as mean ± s.d. (n = 5).

lung cancer in more *in vivo*-like conditions. Due to its versatility, this enabling technology can also be used to study different combinations of cell populations and more complex ECM domains can be easily included, thus allowing to evaluate their specific functions and effects in cancer cells survival with different treatments.

Acknowledgments

The authors would like to acknowledge the support of the European Research Council grant agreement ERC-2014-ADG-669858 for project "ATLAS". The authors also acknowledge the financial support by the

Portuguese Foundation for Science and Technology (FCT) through a Post-doctoral grant (SFRH/BPD/119983/2016, Vítor Gaspar). This work was also developed within the scope of the project CICECO - Aveiro Institute of Materials, POCI-01-0145-FEDER-007679 (FCT Ref. UID/CTM/50011/2013), financed by national funds through the FCT/MEC and when appropriate co-financed by FEDER under the PT2020 Partnership Agreement.

Appendix A. Supplementary data

Supplementary data to this article can be found online at https://doi.org/10.1016/j.biomaterials.2018.09.007.

References

[1] B.A. Ruggeri, F. Camp, S. Miknyoczki, Animal models of disease: pre-clinical animal models of cancer and their applications and utility in drug discovery, Biochem. Pharmacol. 87 (2014) 150–161, https://doi.org/10.1016/j.bcp.2013.06.020.
[2] R.H. Shoemaker, The NCI60 human tumour cell line anticancer drug screen, Nat. Rev. Canc. 6 (2006) 813–823, https://doi.org/10.1038/nrc1951.
[3] A. Nyga, U. Cheema, M. Loizidou, 3D tumour models: novel in vitro approaches to cancer studies, J. Cell Commun. Signal. 5 (2011) 239–248, https://doi.org/10.1007/s12079-011-0132-4.
[4] S. Breslin, L. O'Driscoll, Three-dimensional cell culture: the missing link in drug discovery, Drug Discov. Today 18 (2013) 240–249, https://doi.org/10.1016/j.drudis.2012.10.003.
[5] F. Pampaloni, E.G. Reynaud, E.H.K. Stelzer, The third dimension bridges the gap between cell culture and live tissue, Nat. Rev. Mol. Cell Biol. 8 (2007) 839–845, https://doi.org/10.1038/nrm2236.
[6] S. Aparicio, M. Hidalgo, A.L. Kung, Examining the utility of patient-derived xenograft mouse models, Nat. Rev. Canc. 15 (2015) 311–316, https://doi.org/10.1038/nrc3944.
[7] J.W. Cassidy, C. Caldas, A. Bruna, Europe PMC funders group maintaining tumour heterogeneity in patient-derived, Tumour Xenografts 75 (2016) 2963–2968, https://doi.org/10.1158/0008-5472.CAN-15-0727 (Maintaining).
[8] C.R. Thoma, M. Zimmermann, I. Agarkova, J.M. Kelm, W. Krek, 3D cell culture systems modeling tumor growth determinants in cancer target discovery, Adv. Drug Deliv. Rev. 69–70 (2014) 29–41, https://doi.org/10.1016/j.addr.2014.03.001.
[9] G. Lazzari, P. Couvreur, S. Mura, Multicellular tumor spheroids: a relevant 3D model for the in vitro preclinical investigation of polymer nanomedicines, Polym. Chem. 8 (2017) 4947–4969, https://doi.org/10.1039/C7PY00559H.
[10] L.B. Weiswald, D. Bellet, V. Dangles-Marie, Spherical cancer models in tumor biology, Neoplasia 17 (2015) 1–15, https://doi.org/10.1016/j.neo.2014.12.004.
[11] A. Astashkina, D.W. Grainger, Critical analysis of 3-D organoid in vitro cell culture models for high-throughput drug candidate toxicity assessments, Adv. Drug Deliv. Rev. 69–70 (2014) 1–18, https://doi.org/10.1016/j.addr.2014.02.008.
[12] F.M. Kievit, S.J. Florczyk, M.C. Leung, K. Wang, J.D. Wu, J.R. Silber, R.G. Ellenbogen, J.S.H. Lee, M. Zhang, Proliferation and enrichment of CD133+ glioblastoma cancer stem cells on 3D chitosan-alginate scaffolds, Biomaterials 35 (2014) 9137–9143, https://doi.org/10.1016/j.biomaterials.2014.07.037.
[13] L.K. Ferrarelli, Cancer reactivated by collagen, Sci. Signal. 9 (2016), https://doi.org/10.1126/scisignal.aah5670 ec165-ec165.
[14] F. Del Bufalo, T. Manzo, V. Hoyos, S. Yagyu, I. Caruana, J. Jacot, O. Benavides, D. Rosen, M.K. Brenner, 3D modeling of human cancer: a PEG-fibrin hydrogel system to study the role of tumor microenvironment and recapitulate the in vivo effect of oncolytic adenovirus, Biomaterials 84 (2016) 76–85, https://doi.org/10.1016/j.biomaterials.2016.01.030.
[15] A.W. Holle, J.L. Young, J.P. Spatz, In vitro cancer cell-ECM interactions inform in vivo cancer treatment, Adv. Drug Deliv. Rev. 97 (2016) 270–279, https://doi.org/10.1016/j.addr.2015.10.007.
[16] P. Jiang, X. Li, C.B. Thompson, Z. Huang, F. Araiza, R. Osgood, G. Wei, M. Feldmann, G.I. Frost, H.M. Shepard, Effective targeting of the tumor microenvironment for cancer therapy, Anticancer Res. 32 (2012) 1203–1212.
[17] R. Pirinen, R. Tammi, M. Tammi, P. Hirvikoski, J.J. Parkkinen, R. Johansson, J. Böhm, S. Hollmén, V.M. Kosma, Prognostic value of hyaluronan expression in non-small-cell lung cancer: increased stromal expression indicates unfavorable outcome in patients with adenocarcinoma, Int. J. Canc. 95 (2001) 12–17, https://doi.org/10.1002/1097-0215(20010120)95:1<12::AID-IJC1002>3.0.CO;2-E.
[18] R. Stern, Hyaluronan metabolism: a major paradox in cancer biology, Pathol. Biol. 53 (2005) 372–382, https://doi.org/10.1016/j.patbio.2004.12.021.
[19] M.P. Carvalho, E.C. Costa, S.P. Miguel, I.J. Correia, Tumor spheroid assembly on hyaluronic acid-based structures: a review, Carbohydr. Polym. 150 (2016) 139–148, https://doi.org/10.1016/j.carbpol.2016.05.005.
[20] C. Tolg, J.B. McCarthy, A. Yazdani, E.A. Turley, Hyaluronan and RHAMM in wound repair and the "cancerization" of stromal tissues, BioMed Res. Int. 2014 (2014) 1–18, https://doi.org/10.1155/2014/103923.
[21] A.-P. Morel, M. Lièvre, C. Thomas, G. Hinkal, S. Ansieau, A. Puisieux, Generation of breast cancer stem cells through epithelial-mesenchymal transition, PLoS One 3 (2008) e2888, https://doi.org/10.1371/journal.pone.0002888.
[22] W. Cheng, T. Liu, X. Wan, Y. Gao, H. Wang, MicroRNA-199a targets CD44 to suppress the tumorigenicity and multidrug resistance of ovarian cancer-initiating cells, FEBS J. 279 (2012) 2047–2059, https://doi.org/10.1111/j.1742-4658.2012.08589.x.
[23] F. Cammarota, M.O. Laukkanen, Mesenchymal stem/stromal cells in stromal evolution and cancer progression, Stem Cell. Int. 2016 (2016), https://doi.org/10.1155/2016/4824573.
[24] T. Lopatina, C. Gai, M.C. Deregibus, S. Kholia, G. Camussi, Cross talk between cancer and mesenchymal stem cells through extracellular vesicles carrying nucleic acids, Front. Oncol. 6 (2016) 125, https://doi.org/10.3389/fonc.2016.00125.
[25] S.M. Ridge, F.J. Sullivan, S.A. Glynn, Mesenchymal stem cells: key players in cancer progression, Mol. Canc. 16 (2017) 31, https://doi.org/10.1186/s12943-017-0597-8.
[26] L. Gwendal, L. Paula Y, G. Lazennec, P.Y. Lam, Recent discoveries concerning the tumor - mesenchymal stem cell interactions, Biochim. Biophys. Acta Rev. Canc 1866 (2016) 290–299, https://doi.org/10.1016/j.bbcan.2016.10.004.
[27] M. Gazdic, B. Simovic Markovic, N. Jovicic, M. Misirkic-Marjanovic, V. Djonov, V. Jakovljevic, N. Arsenijevic, M.L. Lukic, V. Volarevic, Mesenchymal stem cells promote metastasis of lung cancer cells by downregulating systemic antitumor immune response, Stem Cell. Int. 2017 (2017), https://doi.org/10.1155/2017/6294717.
[28] Y. Lu, J. Liu, Y. Liu, Y. Qin, Q. Luo, Q. Wang, H. Duan, TLR4 plays a crucial role in MSC-induced inhibition of NK cell function, Biochem. Biophys. Res. Commun. 464 (2015) 541–547, https://doi.org/10.1016/j.bbrc.2015.07.002.
[29] C. Choe, Y.S. Shin, S.H. Kim, M.J. Jeon, S.J. Choi, J. Lee, J. Kim, Tumor-stromal interactions with direct cell contacts enhance motility of non-small cell lung cancer cells through the hedgehog signaling pathway, Anticancer Res. 33 (2013) 3715–3724, https://doi.org/10.1016/B978-0-12-386469-7.00001-3.
[30] R. Liu, S. Wei, J. Chen, S. Xu, Mesenchymal stem cells in lung cancer tumor microenvironment: their biological properties, influence on tumor growth and therapeutic implications, Canc. Lett. 353 (2014) 145–152, https://doi.org/10.1016/j.canlet.2014.07.047.
[31] S. Gottschling, M. Granzow, R. Kuner, A. Jauch, E. Herpel, E.C. Xu, T. Muley, P.A. Schnabel, F.J.F. Herth, M. Meister, Mesenchymal stem cells in non-small cell lung cancer-Different from others? Insights from comparative molecular and functional analyses, Lung Canc. 80 (2013) 19–29, https://doi.org/10.1016/j.lungcan.2012.12.015.
[32] M.H. Xu, X. Gao, D. Luo, X.D. Zhou, W. Xiong, G.X. Liu, EMT and acquisition of stem cell-like properties are involved in spontaneous formation of tumorigenic hybrids between lung cancer and bone marrow-derived mesenchymal stem cells, PLoS One 9 (2014), https://doi.org/10.1371/journal.pone.0087893.
[33] F. Norozi, A. Ahmadzadeh, S. Shahrabi, T. Vosoughi, N. Saki, Mesenchymal stem cells as a double-edged sword in suppression or progression of solid tumor cells, Tumor Biol. 37 (2016) 11679–11689, https://doi.org/10.1007/s13277-016-5187-7.
[34] L.P. Ferreira, V.M. Gaspar, R. Henrique, C. Jerónimo, J.F. Mano, Mesenchymal stem cells relevance in multicellular bioengineered 3D in vitro tumor models, Biotechnol. J. 12 (2017) 1700079, , https://doi.org/10.1002/biot.201700079.
[35] C.A. Schneider, W.S. Rasband, K.W. Eliceiri, NIH Image to ImageJ: 25 years of image analysis, Nat. Methods 9 (2012) 671–675, https://doi.org/10.1038/nmeth.2089.
[36] N. Baek, O.W. Seo, M. Kim, J. Hulme, S.S.A. An, Monitoring the effects of doxorubicin on 3D-spheroid tumor cells in real-time, OncoTargets Ther. 9 (2016) 7207–7218, https://doi.org/10.2147/OTT.S112566.
[37] E.C. Costa, V.M. Gaspar, P. Coutinho, I.J. Correia, Optimization of liquid overlay technique to formulate heterogenic 3D co-cultures models, Biotechnol. Bioeng. 111 (2014) 1672–1685, https://doi.org/10.1002/bit.25210.
[38] J.G. Delinasios, F. Angeli, G. Koumakis, S. Kumar, W.H. Kang, G. Sica, F. Iacopino, G. Lama, S. Lamprecht, I. Sigal-Batikoff, G.T. Tsangaris, C.D. Farfarelos, M.C. Farfarelos, E. Vairaktaris, S. Vassiliou, G.J. Delinasios, Proliferating fibroblasts and HeLa cells co-cultured in vitro reciprocally influence growth patterns, protein expression, chromatin features and cell survival, Anticancer Res. 35 (2015) 1881–1916.
[39] E.L.S. Fong, D.A. Harrington, M.C. Farach-Carson, H. Yu, Heralding a new paradigm in 3D tumor modeling, Biomaterials 108 (2016) 197–213, https://doi.org/10.1016/j.biomaterials.2016.08.052.
[40] A. Amann, M. Zwierzina, G. Gamerith, M. Bitsche, J.M. Huber, G.F. Vogel, M. Blumer, S. Koeck, E.J. Pechriggl, J.M. Kelm, W. Hilbe, H. Zwierzina, Development of an innovative 3D cell culture system to study tumour - stroma interactions in non-small cell lung cancer cells, PLoS One 9 (2014), https://doi.org/10.1371/journal.pone.0092511.
[41] G.J. Block, S. Ohkouchi, F. Fung, J. Frenkel, C. Gregory, R. Pochampally, G. DiMattia, D.E. Sullivan, D.J. Prockop, Multipotent stromal cells are activated to reduce apoptosis in part by upregulation and secretion of stanniocalcin-1, Stem Cell. 27 (2009) 670–681, https://doi.org/10.1002/stem.20080742.Multipotent.
[42] X. Ji, J. Ji, F. Shan, Y. Zhang, Y. Chen, X. Lu, Cancer-associated fibroblasts from NSCLC promote the radioresistance in lung cancer cell lines, Int. J. Clin. Exp. Med. 8 (2015) 7002–7008.
[43] D.P. Ivanov, T.L. Parker, D.A. Walker, C. Alexander, M.B. Ashford, P.R. Gellert, M.C. Garnett, Multiplexing spheroid volume, resazurin and acid phosphatase viability assays for high-throughput screening of tumour spheroids and stem cell neurospheres, PLoS One 9 (2014) 1–14, https://doi.org/10.1371/journal.pone.0103817.
[44] H. Hardelauf, J.-P. Frimat, J.D. Stewart, W. Schormann, Y.-Y. Chiang, P. Lampen, J. Franzke, J.G. Hengstler, C. Cadenas, L.A. Kunz-Schughart, Microarrays for the scalable production of metabolically relevant tumour spheroids: a tool for modulating chemosensitivity traits, Lab a Chip 11 (2011) 419–428.
[45] Y.-R. Lou, L. Kanninen, B. Kaehr, J.L. Townson, J. Niklander, R. Harjumäki,

C. Jeffrey Brinker, M. Yliperttula, Silica bioreplication preserves three-dimensional spheroid structures of human pluripotent stem cells and HepG2 cells, Sci. Rep. 5 (2015) 13635, https://doi.org/10.1038/srep13635.
[46] M. Ma, J. Xu, W.M. Purcell, Biochemical and functional changes of rat liver spheroids during spheroid formation and maintenance in culture: I. Morphological maturation and kinetic changes of energy metabolism, albumin synthesis, and activities of some enzymes, J. Cell. Biochem. 90 (2003) 1166–1175, https://doi.org/10.1002/jcb.10730.
[47] M.C. Cox, L.M. Reese, L.R. Bickford, S.S. Verbridge, Toward the broad adoption of 3D tumor models in the cancer drug pipeline, ACS Biomater. Sci. Eng. 1 (2015) 877–894, https://doi.org/10.1021/acsbiomaterials.5b00172.
[48] V. Brancato, A. Garziano, F. Gioiella, F. Urciuolo, G. Imparato, V. Panzetta, S. Fusco, P.A. Netti, 3D is not enough: Building up a cell instructive microenvironment for tumoral stroma microtissues, Acta Biomater. 47 (2017) 1–13, https://doi.org/10.1016/j.actbio.2016.10.007.
[49] C.C. Ahrens, Z. Dong, W. Li, Engineering cell aggregates through incorporated polymeric microparticles, Acta Biomater. 62 (2017) 64–81, https://doi.org/10.1016/j.actbio.2017.08.003.
[50] L.P. Ferreira, V.M. Gaspar, J.F. Mano, Design of spherically structured 3D in vitro tumor models -advances and prospects, Acta Biomater. 75 (2018) 11–34, https://doi.org/10.1016/j.actbio.2018.05.034.
[51] F. Augustin, M. Fiegl, T. Schmid, G. Pomme, W. Sterlacci, A. Tzankov, Receptor for hyaluronic acid-mediated motility (RHAMM, CD168) expression is prognostically important in both nodal negative and nodal positive large cell lung cancer, J. Clin. Pathol. 68 (2015) 368–373, https://doi.org/10.1136/jclinpath-2014-202819.
[52] A. Khademhosseini, K.Y. Suh, J.M. Yang, G. Eng, J. Yeh, S. Levenberg, R. Langer, Layer-by-layer deposition of hyaluronic acid and poly-L-lysine for patterned cell co-cultures, Biomaterials 25 (2004) 3583–3592, https://doi.org/10.1016/j.biomaterials.2003.10.033.
[53] S. Kumar, Cellular mechanotransduction: stiffness does matter, Nat. Mater. 13 (2014) 918–920, https://doi.org/10.1038/nmat4094.
[54] E. Fennema, N. Rivron, J. Rouwkema, C. van Blitterswijk, J. De Boer, Spheroid culture as a tool for creating 3D complex tissues, Trends Biotechnol. 31 (2013) 108–115, https://doi.org/10.1016/j.tibtech.2012.12.003.
[55] G.L. Semenza, The hypoxic tumor microenvironment: a driving force for breast cancer progression, Biochim. Biophys. Acta Mol. Cell Res. 1863 (2016) 382–391, https://doi.org/10.1016/j.bbamcr.2015.05.036.
[56] M. Zanoni, F. Piccinini, C. Arienti, A. Zamagni, S. Santi, R. Polico, A. Bevilacqua, A. Tesei, 3D tumor spheroid models for in vitro therapeutic screening: a systematic approach to enhance the biological relevance of data obtained, Sci. Rep. 6 (2016) 19103, https://doi.org/10.1038/srep19103.
[57] A. Dittmer, A. Fuchs, I. Oerlecke, B. Leyh, S. Kaiser, J.W.M. Martens, J. L??tzkendorf, L. M??ller, J. Dittmer, Mesenchymal stem cells and carcinoma-associated fibroblasts sensitize breast cancer cells in 3D cultures to kinase inhibitors, Int. J. Oncol. 39 (2011) 689–696, https://doi.org/10.3892/ijo.2011.1073.
[58] H.K. Eltzschig, P. Carmeliet, Hypoxia and inflammation, N. Engl. J. Med. 364 (2011) 1976–1977, https://doi.org/10.1056/NEJMra0910283.
[59] S.J. Grainger, A.J. Putnam, Assessing the permeability of engineered capillary networks in a 3D culture, PLoS One 6 (2011), https://doi.org/10.1371/journal.pone.0022086.
[60] D. Keskin, J. Kim, V.G. Cooke, C.C. Wu, H. Sugimoto, C. Gu, M. De Palma, R. Kalluri, V.S. LeBleu, Targeting vascular pericytes in hypoxic tumors increases lung metastasis via Angiopoietin-2, Cell Rep. 10 (2015) 1066–1081, https://doi.org/10.1016/j.celrep.2015.01.035.
[61] A. Dittmer, K. Hohlfeld, J. Lützkendorf, L.P. Müller, J. Dittmer, Human mesenchymal stem cells induce E-cadherin degradation in breast carcinoma spheroids by activating ADAM10, Cell. Mol. Life Sci. 66 (2009) 3053–3065, https://doi.org/10.1007/s00018-009-0089-0.
[62] W.H. Koppenol, P.L. Bounds, C.V. Dang, Otto Warburg's contributions to current concepts of cancer metabolism, Nat. Rev. Canc. 11 (2011) 325–337, https://doi.org/10.1038/nrc3038.
[63] R. Derda, A. Laromaine, A. Mammoto, S.K.Y. Tang, T. Mammoto, D.E. Ingber, G.M. Whitesides, Paper-supported 3D cell culture for tissue-based bioassays, Proc. Natl. Acad. Sci. 106 (2009) 18457–18462, https://doi.org/10.1073/pnas.0910666106.
[64] I. Hughes, B. Blasiole, D. Huss, M.E. Warchol, N.P. Rath, B. Hurle, E. Ignatova, J. David Dickman, R. Thalmann, R. Levenson, D.M. Ornitz, The tumor microenvironment in non-small cell lung cancer, Dev. Biol. 276 (2004) 391–402, https://doi.org/10.1016/j.semradonc.2010.01.003.
[65] P. Chaturvedi, D.M. Gilkes, C. Chak, L. Wong, W. Luo, H. Zhang, H. Wei, N. Takano, L. Schito, A. Levchenko, G.L. Semenza, Hypoxia-inducible factor – dependent breast cancer – mesenchymal stem cell bidirectional signaling promotes metastasis, J. Clin. Invest. 123 (2013) 189–205, https://doi.org/10.1172/JCI64993DS1.
[66] T.R. Olsen, B. Mattix, M. Casco, A. Herbst, C. Williams, A. Tarasidis, G. Evans, L. Jenkins, C.L. McMahan, D. Simionescu, R.P. Visconti, F. Alexis, Processing cellular spheroids for histological examination, J. Histotechnol. 37 (2014) 138–142, https://doi.org/10.1179/2046023614Y.0000000047.
[67] M. Fang, J. Yuan, C. Peng, Y. Li, Collagen as a double-edged sword in tumor progression, Tumor Biol. 35 (2014) 2871–2882, https://doi.org/10.1007/s13277-013-1511-7.
[68] Z. Chen, C.M. Fillmore, P.S. Hammerman, C.F. Kim, K.-K.K. Wong, Non-small-cell lung cancers: a heterogeneous set of diseases, Nat. Rev. Canc. 15 (2015), https://doi.org/10.1038/nrc3931 247–247.
[69] C.E. Barcus, K.A. O'Leary, J.L. Brockman, D.E. Rugowski, Y. Liu, N. Garcia, M. Yu, P.J. Keely, K.W. Eliceiri, L.A. Schuler, Elevated collagen-I augments tumor progressive signals, intravasation and metastasis of prolactin-induced estrogen receptor alpha positive mammary tumor cells, Breast Cancer Res. 19 (2017) 9, https://doi.org/10.1186/s13058-017-0801-1.
[70] L. Stone, Prostate cancer: a glitch in the extracellular matrix, Nat. Rev. Urol. 14 (2017) 8, https://doi.org/10.1038/nrurol.2016.238.
[71] K.M. Riching, B.L. Cox, M.R. Salick, C. Pehlke, A.S. Riching, S.M. Ponik, B.R. Bass, W.C. Crone, Y. Jiang, A.M. Weaver, K.W. Eliceiri, P.J. Keely, 3D collagen alignment limits protrusions to enhance breast cancer cell persistence, Biophys. J. 107 (2015) 2546–2558, https://doi.org/10.1016/j.bpj.2014.10.035.
[72] S. Misra, V.C. Hascall, R.R. Markwald, S. Ghatak, Interactions between hyaluronan and its receptors (CD44, RHAMM) regulate the activities of inflammation and cancer, Front. Immunol. 6 (2015), https://doi.org/10.3389/fimmu.2015.00201.
[73] K. Wang, F.M. Kievit, A.E. Erickson, J.R. Silber, R.G. Ellenbogen, M. Zhang, Culture on 3D chitosan-hyaluronic acid scaffolds enhances stem cell marker expression and drug resistance in human glioblastoma cancer stem cells, Adv. Healthc. Mater. 5 (2016) 3173–3181, https://doi.org/10.1002/adhm.201600684.
[74] C.W. Tsai, T.H. Young, CD44 expression trends of mesenchymal stem-derived cell, cancer cell and fibroblast spheroids on chitosan-coated surfaces, Pure Appl. Chem. 88 (2016) 843–852, https://doi.org/10.1515/pac-2016-0405.
[75] E.L.-H. Leung, R.R. Fiscus, J.W. Tung, V.P.-C. Tin, L.C. Cheng, A.D.-L. Sihoe, L.M. Fink, Y. Ma, M.P. Wong, Non-Small Cell Lung Cancer Cells Expressing CD44 Are Enriched for Stem Cell-Like Properties, PLoS One 5 (2010) e14062, , https://doi.org/10.1371/journal.pone.0014062.
[76] Y. Zhang, Z. Zhang, Q. Guan, Y. Liu, Z. Wu, J. Li, Y. Su, C. Yan, Y. Luo, J. Qin, Q. Wang, X. Xie, Co-culture with lung cancer A549 cells promotes the proliferation and migration of mesenchymal stem cells derived from bone marrow, Exp. Ther. Med. (2017) 2983–2991, https://doi.org/10.3892/etm.2017.4909.
[77] J. Tao, N. Ybarra, I. El Naqa, A549 lung cancer cells up-regulate proto-oncogene expression in mesenchymal stem cells, Int. J. Radiat. Oncol. 90 (2014) S770, https://doi.org/10.1016/j.ijrobp.2014.05.2229.
[78] Y. Shi, L. Du, L. Lin, Y. Wang, Tumour-associated mesenchymal stem/stromal cells: emerging therapeutic targets, Nat. Rev. Drug Discov. 16 (2016) 35–52, https://doi.org/10.1038/nrd.2016.193.
[79] H.-W. Han, S. Hsu, Chitosan-hyaluronan based 3D co-culture platform for studying the crosstalk of lung cancer cells and mesenchymal stem cells, Acta Biomater. 42 (2016) 157–167, https://doi.org/10.1016/j.actbio.2016.06.014.
[80] M. Probes, Vybrant cell-labeling solutions, Solutions (2001) 1–3.
[81] R.F. Foronjy, S.M. Majka, The potential for resident lung mesenchymal stem cells to promote functional tissue regeneration: understanding microenvironmental cues, Cells 1 (2012) 874–885.
[82] A. Nowakowski, K. Drela, J. Rozycka, M. Janowski, B. Lukomska, Engineered mesenchymal stem cells as an anti-cancer trojan horse, Stem Cell. Dev. 25 (2016) 1513–1531, https://doi.org/10.1089/scd.2016.0120.
[83] S.L. Wood, M. Pernemalm, P.A. Crosbie, A.D. Whetton, The role of the tumor-microenvironment in lung cancer-metastasis and its relationship to potential therapeutic targets, Canc. Treat Rev. 40 (2014) 558–566, https://doi.org/10.1016/j.ctrv.2013.10.001.
[84] G. Szakács, J.K. Paterson, J.A. Ludwig, C. Booth-Genthe, M.M. Gottesman, Targeting multidrug resistance in cancer, Nat. Rev. Drug Discov. 5 (2006) 219–234, https://doi.org/10.1038/nrd1984.
[85] W.-T, Hopper-Borge, Drug resistance mechanisms in non-small cell lung carcinoma, J Can Res Updat 2 (2014) 265–282, https://doi.org/10.6000/1929-2279.2013.02.04.5.Drug.
[86] A. Östman, M. Augsten, Cancer-associated fibroblasts and tumor growth - bystanders turning into key players, Curr. Opin. Genet. Dev. 19 (2009) 67–73, https://doi.org/10.1016/j.gde.2009.01.003.
[87] Y. Shintani, A. Abulaiti, T. Kimura, S. Funaki, T. Nakagiri, M. Inoue, N. Sawabata, M. Minami, E. Morii, M. Okumura, Pulmonary fibroblasts induce epithelial mesenchymal transition and some characteristics of stem cells in non-small cell lung cancer, Ann. Thorac. Surg. 96 (2013) 425–433, https://doi.org/10.1016/j.athoracsur.2013.03.092.